NASA Technical Paper 2906

1989

The Effects of Simulated Space Environmental Parameters on Six Commercially Available Composite Materials

Joan G. Funk and
George F. Sykes, Jr.
Langley Research Center
Hampton, Virginia

National Aeronautics and Space Administration
Office of Management
Scientific and Technical Information Division

The use of trademarks or names of manufacturers in this report is for accurate reporting and does not constitute an official endorsement, either expressed or implied, of such products or manufacturers by the National Aeronautics and Space Administration.

Abstract

The effects of simulated space environmental parameters on microdamage induced by the environment in a series of commercially available graphite-fiber-reinforced composite materials were determined. Composites with both thermoset and thermoplastic resin systems were studied. Low-Earth-orbit (LEO) exposures were simulated by thermal cycling; geosynchronous-orbit (GEO) exposures were simulated by electron irradiation plus thermal cycling. The thermal cycling temperature range was −250°F to either 200°F or 150°F. The upper limits of the thermal cycles were different to ensure that an individual composite material was not cycled above its glass transition temperature. Material response was characterized through assessment of the induced microcracking and its influence on mechanical property changes at both room temperature and −250°F. Microdamage was induced in both thermoset and thermoplastic advanced composite materials exposed to the simulated LEO environment. However, a 350°F-cure single-phase toughened epoxy composite was not damaged during exposure to the LEO environment. The simulated GEO environment produced microdamage in all materials tested.

Introduction

Graphite-fiber-reinforced polymer-matrix composite materials are being considered for structural applications in many future spacecraft, including the Space Station Freedom and planned precision geostationary reflectors and antennas (refs. 1 and 2). These materials are attractive for space applications because of their low density, high strength, stiffness, and dimensional stability. They have exhibited good environmental durability in previous short term (<3 years) space applications. However, because most future spacecraft will be designed for missions longer than 10 years, there is concern that the space environment may interact with the polymer matrix to alter the attractive properties of the composites.

A primary concern is the sensitivity of these materials to microcracking during exposure to the thermal cycling conditions which are characteristic of both low-Earth-orbit (LEO) and geosynchronous-orbit (GEO) environments. Microdamage resulting from this thermal cycling has been reported for many widely used aerospace polymer-matrix composites (refs. 3 and 4). In addition, it has been shown that, when combined with the ionizing radiation component typical of GEO, microdamage induced by thermal cycling is significantly increased (ref. 5). Since microdamage may affect important design properties (and thus spacecraft performance), techniques for reducing the sensitivity of composites to microcracking induced by thermal cycling are being examined (ref. 6).

In the study report herein, the durability in simulated LEO and GEO thermal cycling environments of six commercially available aerospace composite materials was determined. The response was characterized by determination of the microdamage resulting from thermal cycling or from electron irradiation followed by thermal cycling and the influence of the exposure on the mechanical properties of the material.

Materials and Test Procedures

The graphite-fiber-reinforced composite materials used in this study are listed in table I. The prepreg source and a brief description of the matrix of each material are given. The exact composition of most of these materials is proprietary, and therefore they are described here in only general terms. The matrices evaluated included an amorphous thermoplastic (C6000/P1700), two semicrystalline thermoplastics (AS4/PPS and AS4/PEEK), a 250°F-cure two-phase epoxy (T300/CE339), a 350°F-cure single-phase toughened epoxy (T300/BP907), and a 350°F-cure single-phase epoxy (T300/934). This group of materials was selected to provide a relatively wide range of matrix properties. The three fibers used in this study, C6000, AS4, and T300, are polyacrylonitrile- (PAN-) based graphite fibers with a tensile modulus of about 33×10^6 psi.

All the materials, except the two semicrystalline thermoplastics, were produced from unidirectional prepreg tape purchased from the indicated manufacturers. The prepreg was used to prepare eight-ply quasi-isotropic $[0, \pm 45, 90]_s$ panels which were autoclave cured using the manufacturers' established processing cycle. The two semicrystalline materials were supplied by the indicated manufacturer as finished $[0, \pm 45, 90]_s$ panels. The nominal thicknesses of the panels ranged from 0.043 to 0.051 in. Characteristics of the laminates shown in table II indicate that all materials had about the same fiber volume fraction. The fiber volume fraction of the AS4/PEEK composite was not obtainable with the acid digestion procedure used for all other materials because of the insolubility of PEEK in nitric acid. However, the density and volatile content are listed in table II.

The laminates were machined into test specimens and tested in the as-fabricated condition and after exposure to thermal cycling or to radiation followed by thermal cycling. Specimens for tensile testing and microcrack analysis were 0.5 in. wide and

6.0 in. long. Specimens for thermomechanical analysis (TMA) were 0.25 in. by 0.25 in.

All specimens were dried for a minimum of 30 days at room temperature in vacuum before testing. Following thermal cycling, strain gages were bonded to the center and fiberglass tabs were bonded to the end of each tensile test specimen. The fiberglass tabs, bonded with a room temperature curing adhesive, were used to introduce load into the specimen and prevent grip damage.

Thermal Cycling

A dual-chamber exposure unit was used to simulate "worst case" LEO and GEO thermal cycling environments. For the LEO simulation, only the effects of thermal cycling were studied. For the GEO simulation, specimens that had been previously irradiated (as discussed subsequently) were also thermally cycled. In the thermal cycling apparatus, specimens mounted on a mechanically driven tray were alternately moved from a cooled chamber to a heated chamber. Temperature was monitored with a thermocouple attached to the specimen surface. The total time for one cycle was about 28 minutes and the specimens remained in each chamber approximately 10 minutes after reaching ambient temperature.

Two different thermal cycles were used in this study. The lower temperature limit for both thermal cycles was −250°F, but the upper temperature limits were different (see fig. 1). The T300/BP907, AS4/PEEK, C6000/P1700, and T300/934 laminates were exposed to cycle A, which had an upper temperature limit of 200°F. The AS4/PPS and T300/CE339 laminates were exposed to cycle B, which had an upper temperature limit of 150°F. The two cycles were used to ensure that the composite materials were not cycled above their glass transition temperature. The glass transition region for all the materials is shown in figure 2, wherein the results from thermomechanical analysis are given. These data show the softening range associated with the glass transition. The upper thermal cycling temperature is indicated by an arrow on each softening curve. All specimens received 500 thermal cycles in dry nitrogen at atmospheric pressure.

Following thermal cycling, the specimens were examined with X-rays for evidence of cracks. An X-ray opaque penetrant solution (zinc iodide and isopropyl alcohol) was applied to the specimen along the edges and allowed to flow into the cracks for several minutes. Following this soak period, the specimen was wiped clean with a water-dampened cloth and a radiograph of the specimen was made. The magnified X-ray photograph was used to characterize the number of cracks per inch of length of the specimen.

Radiation Exposure

The radiation component of the GEO environment was simulated by exposing the composite specimens to 1 MeV electrons in a clean, turbopumped vacuum exposure chamber at a pressure of 2×10^{-7} torr. Up to 19 specimens were irradiated simultaneously using a Radiation Dynamics, Inc., Dynamitron Model 1000/10 accelerator. The specimens were mounted side by side on a temperature-controlled aluminum mounting plate positioned in the uniform area of the electron beam. The materials received a dose of 1×10^{10} rads at a rate of 5×10^{7} rads/hr without interruption. This total dose is equivalent to approximately 30 years in GEO. The absorbed dose and dose rate were calculated from current flux levels monitored with a Faraday cup mounted in the exposure area of the base plate. The Faraday cup was calibrated through the use of National Bureau of Standards calibrated polymeric dosimeter films. At the dose rate selected, specimen temperature did not exceed 100°F during the radiation exposure. Radiation exposure was conducted on sets of composite material specimens designated for thermomechanical analysis, tensile property evaluation, and thermal cycling experiments.

Tensile Property Testing

The tensile behavior of each composite was characterized by measurement of the stress, strain, and modulus of the $[0, \pm 45, 90]_s$ coupons at both room temperature and −250°F. The ultimate stress and failure strain were determined either at onset of delamination or, in the case of no delamination, at failure. A crosshead loading rate of 0.02 in./min was used for all tests. Stress and strain were calculated and recorded once every second with a data acquisition system that monitored the strain gages located on the test specimens and the load cell of the test machine.

Thermomechanical Analysis

Thermomechanical analyses of all materials were performed with a Du Pont Co. model 943 Thermomechanical Analyzer. Out-of-plane laminate expansion or penetration was performed on 0.25-in. by 0.25-in. specimens with the TMA accessory. In this test, the movement of a 0.125-in-diameter, hemispherical-tipped quartz probe resting on the specimen was monitored as the specimen was heated from room temperature through its softening range.

Results and Discussion

The TMA data, microcrack density, and mechanical property data for each material are presented in

figures 3 to 38. The data for each material will be discussed separately. Table III and figures 39 to 44 compile the results for the different materials and allow comparisons of the material properties.

T300/934

The T300/934 TMA data are shown in figure 3 and the microcrack density is shown in figure 4. Typical stress-strain curves for T300/934 are shown in figure 5. The modulus, ultimate strength, and failure strain for T300/934 are shown in figures 6 to 8. The lowest test temperature resulted in a decrease in the strength and strain of the baseline material. The lowest test temperature caused higher residual stresses than did the room temperature test, and this increase is reflected in the decrease in the ultimate properties of the material.

Thermal cycling and the resulting microcrack density of 18 cracks/in. did not significantly change the mechanical properties at either room temperature or −250°F. The glass transition temperature T_g of the material was not affected by the thermal cycling exposure. Irradiation followed by thermal cycling, which resulted in a crack density of 43 cracks/in., reduced the ultimate strength and failure strain at both test temperatures, particularly at −250°F, and reduced the T_g of the material.

As described in reference 7, at and below room temperature the epoxy resin becomes stiffer and more brittle following irradiation. In reference 7, the modulus of the matrix-dominated laminates ($[90]_4$) increased while the ultimate strength decreased. Lower residual stresses (caused by the electron irradiation interaction, which breaks some of the bonds within the epoxy structure) result in straighter fibers, thereby giving the irradiated material a higher modulus than that of the nonirradiated material.

The room-temperature T300/934 data presented in this paper show a similar trend in that the ultimate strength of the quasi-isotropic laminate decreased with irradiation followed by thermal cycling. However, the modulus for the room-temperature test specimens also decreased. Unlike the aforementioned data in reference 7, which are for irradiated 90° specimens, the quasi-isotropic specimens in the present study were thermal cycled after irradiation. The microcracking resulting from the radiation and thermal exposures contributed to the decrease in the modulus, strength, and strain of the material.

T300/BP907

The T300/BP907 TMA data are shown in figure 9 and the microcrack density is shown in figure 10. Typical stress-strain curves for T300/BP907 are shown in figure 11. The modulus, ultimate strength, and failure strain are shown in figures 12 to 14. The ultimate strength and failure strain used in these figures for the irradiated and thermal cycled material are the failure strength and strain to failure of the material, since this material was already extensively delaminated prior to testing. The modulus and the failure strain could not be determined at the −250°F test temperature because of the delamination of the material. The reduction from room temperature to −250°F did not significantly affect the mechanical properties of the baseline material.

The exposure to thermal cycling, which resulted in no microcracking, did not change the mechanical properties of the material. The T_g increased with thermal cycling, an indication that additional curing possibly occurred at the elevated temperature portion of the thermal cycle. A similar trend has been observed during isothermal aging of other epoxy systems (ref. 8). The method of achieving toughness through incorporating flexible segments into the relatively brittle epoxy chemistry provides durability up to the 500 thermal cycles used in this study.

The irradiation followed by thermal cycling exposure resulted in significant delamination and microcracking. The extensive delamination and microcracking prevented a measurement of the modulus and failure strain at the −250°F test temperature. The decrease in T_g and extension of the softening range may indicate that chain scission was the primary radiation interaction mechanism. The high amount of microcracking and delamination resulted in significant reduction in the mechanical properties of this material.

T300/CE339

The T300/CE339 TMA data are shown in figure 15 and the microcrack density is shown in figure 16. Typical stress-strain curves for T300/CE339 are shown in figure 17. The modulus, ultimate strength, and failure strain are shown in figures 18 to 20. The T_g of the material did not change with exposure to thermal cycling or irradiation followed by thermal cycling. The ultimate strength and failure strain of the irradiated and thermal cycled material are the failure strength and the failure strain of the material. The mechanical properties of the baseline material remained the same as the test temperature was lowered. After 500 thermal cycles the microcrack density of the material had increased to 20 cracks/in. However, the increase in microcrack density did not result in a significant decrease in the mechanical properties of the material. The presence of microcracks suggests that achieving toughness through the addition of an elastomeric second

phase does not improve the resistance of the material to microcracking.

The microcrack density increased to 64 cracks/in. when the material was irradiated and subsequently thermal cycled. A previous study (ref. 5) suggests that penetrating electrons interact to degrade and cross-link the matrix material. The electron-radiation-induced degradation and subsequent increase in microcrack density resulted in significant decreases in the mechanical properties of the material. The strength and strain shown in figures 19 and 20 are ultimate values, as the material was extensively cracked prior to testing. The extensive microcracking precluded the determination of the modulus of the material tested at −250°F.

C6000/P1700

The C6000/P1700 TMA data and microcrack density are shown in figures 21 and 22. Typical stress-strain curves for C6000/P1700 are shown in figure 23. The modulus, ultimate strength, and failure strain for C6000/P1700 are shown in figures 24 to 26. The C6000/P1700 thermoplastic system exhibited microcracks in the as-fabricated condition. The possible influence of the X-ray opaque penetrant solution on damage formation in this composite was evaluated by soaking a neat casting of polysulfone in the solution. No cracking or crazing was found, and this suggests that the microdamage observed in the baseline C6000/P1700 laminate was a result of the fabrication or specimen machining procedures. The decrease in test temperature from room temperature to −250°F resulted in an increase in both modulus and ultimate strength of the baseline material.

Exposure to 500 thermal cycles did not alter the T_g of the material. However the thermal cycling exposure significantly increased the microcrack density from 13 to 53 cracks/in. After thermal cycling, the modulus, ultimate strength, and failure strain of the material at −250°F and at room temperature remained constant.

A previous study on the effects of radiation on P1700 film (ref. 9) has shown that low-molecular-weight fragments are produced by radiation exposure. At doses greater than 1×10^9 rads of electron radiation, cross-linking occurs and increases the modulus and T_g of the film. In the present study the microcrack density increased and T_g decreased after exposure to 1×10^{10} rads followed by 500 thermal cycles. At both room temperature and −250°F, the mechanical properties were not significantly altered by the exposure to electron radiation prior to thermal cycling as compared with the properties of the thermal cycled material.

AS4/PPS

The AS4/PPS TMA data and microcrack density are shown in figures 27 and 28. Typical stress-strain curves for AS4/PPS are shown in figure 29. The modulus, ultimate strength, and failure strain for AS4/PPS are shown in figures 30 to 32. The baseline material showed a slight increase in ultimate strength and modulus with decreasing test temperature. After exposure to thermal cycling the material properties remained constant except for a decrease in failure strain at a test temperature of −250°. The increase in microcrack density from 0 to 48 cracks/in. did not significantly affect the modulus or ultimate strength of the material. The TMA data indicate a significant reduction in the degree of softening following thermal cycling. This may indicate that the material was annealed during thermal cycling and may have increased in crystallinity. The T_g value, which reflects only the amorphous phase of the material, did not increase. The values of T_g for the thermal cycled material and for the irradiated and thermal cycled material were determined from the local minima in the expansion-temperature curve.

Following irradiation and thermal cycling, the ultimate strength at room temperature decreased and the failure strain at −250°F increased substantially compared with the values for the material which had only been thermal cycled. The microcrack density also increased, as did the T_g.

AS4/PEEK

The AS4/PEEK TMA data and microcrack density are shown in figures 33 and 34. Typical stress-strain curves of AS4/PEEK are shown in figure 35. The modulus, ultimate strength, and failure strain for AS4/PEEK are shown in figures 36 to 38. The baseline material showed a significant decrease in ultimate strength and failure strain and a slight increase in modulus at −250°F compared with the properties at room temperature. The decrease in baseline properties at −250°F is attributed to the change in failure mode of the material. At −250°F, the material delaminated prior to failure, whereas at room temperature, the material did not delaminate.

Thermal cycling did not significantly alter the material mechanical properties at either room temperature or −250°F. Irradiating the material prior to thermal cycling resulted in a decrease in the failure strength and failure strain and a small increase in modulus at room temperature and a marked increase in failure strength and strain at −250°F. The simulated GEO exposure increased the ultimate strength and failure strain at −250°F to that of the room-temperature material. A previous study (ref. 10) has

indicated that cross-linking in the amorphous phase of the resin is the primary interaction mechanism of electron irradiation and that electron irradiation does not alter the degree of crystallinity of a semicrystalline PEEK film. The change in the mechanical properties at room temperature after irradiation and thermal cycling are consistent with an increase in the cross-link density of the material. The reason for the increase in the ultimate strength and failure strain at −250°F after irradiation and thermal cycling is not readily apparent.

Microdamage Summary

Table III summarizes the microcrack density data for each material at each exposure condition. All the materials except C6000/P1700 contained no microcracks prior to exposure. As previously discussed, the microcracks present in the baseline C6000/P1700 are attributed to fabrication and/or machining processes. The single-phase toughened epoxy composite T300/BP907 was the only material which showed no microcracks after 500 thermal cycles (simulated LEO). The same epoxy composite had the highest crack density when subjected to 1×10^{10} rads of electron radiation prior to thermal cycling (simulated GEO), thus indicating that material systems suitable for a LEO application may not be suitable for a GEO application. The material with the lowest microcrack density after exposure to the simulated GEO environment was AS4/PEEK, a semicrystalline thermoplastic matrix composite.

Mechanical Properties Summary

As previously stated, some of the materials delaminated prior to failure during testing. In general, the materials did not prematurely delaminate in the baseline and thermal cycled conditions when tested at room temperature, with the exception of T300/934, a 350°F-cure epoxy composite. The two toughened epoxy composites T300/BP907 and T300/CE339, as well as the T300/934, did delaminate prior to failure after being exposed to radiation followed by thermal cycling. The two toughened epoxy composites were severely cracked prior to testing after exposure to radiation followed by thermal cycling. At the −250°F test temperature, four of the six materials, the three thermoset resin composites and one thermoplastic resin composite (AS4/PEEK) delaminated prior to failure for all three conditions tested.

Figure 39 summarizes the modulus data from the tests at room temperature of the quasi-isotropic laminates. In general, exposure to the simulated LEO environment did not significantly affect the modulus at room temperature of any of the six materials. Exposure to the simulated GEO environment, however, resulted in a decrease in the modulus for the three epoxy composites and an increase for the amorphous thermoplastic composite (C6000/P1700) and one of the semicrystalline thermoplastic composites (AS4/PEEK). The modulus at room temperature of the other semicrystalline thermoplastic composite (AS4/PPS) was relatively unchanged by the simulated GEO exposure.

The moduli of the materials tested at −250°F are shown in figure 40. In general, the simulated LEO exposure did not significantly change the modulus at −250°F. The two toughened epoxy composites T300/BP907 and T300/CE339 which had been exposed to the simulated GEO environment were so degraded by the exposure as to preclude a measurement of the modulus at −250°F.

The ultimate strengths of the materials at room temperature are shown in figure 41. The simulated LEO exposure did not result in significant changes in the ultimate strength of the materials. All the materials exhibited a decrease in ultimate strength at room temperature after exposure to electron radiation followed by thermal cycling. The two toughened epoxy composites T300/BP907 and T300/CE339 exhibited the largest decrease in ultimate strength with the simulated GEO exposure.

From the comparison of figure 41 with figure 42, the three epoxy composites exhibited the same ultimate strength behavior at −250°F as at room temperature when exposed to the simulated LEO and GEO environments. At −250°F, the two semicrystalline thermoplastics behaved differently than at room temperature. The ultimate strength at −250°F of the AS4/PPS decreased with thermal cycling but did not show an additional decrease in strength when irradiated prior to thermal cycling. The other semicrystalline thermoplastic system, AS4/PEEK, showed no change in ultimate strength at −250°F with the thermal cycling but substantially increased in strength when irradiated prior to thermal cycling.

The failure strain at room temperature of the materials is shown in figure 43. All the materials exhibited slight or no change in failure strain after exposure to the simulated LEO environment. After exposure to the simulated GEO environment, the failure strain of all the materials decreased from that of the baseline materials.

The failure strain of the materials tested at −250°F is shown in figure 44. The failure strain of the three epoxy composites after exposure to the simulated LEO environment showed little or no change compared with that of the baseline material. The

failure strain of the three epoxy systems decreased markedly after exposure to the simulated GEO environment. The failure strain at −250°F of the amorphous thermoplastic composite C6000/P1700 did not change significantly with exposure to either the simulated LEO or GEO environments. The failure strain at −250°F of the AS4/PPS semicrystalline thermoplastic composite decreased with exposure to the simulated LEO environment. The irradiation exposure prior to thermal cycling increased the failure strain of the AS4/PPS compared with the thermal cycling simulated LEO exposure. The other semicrystalline material, AS4/PEEK, had a significant increase in failure strain (well above that of the baseline material) after exposure to the simulated GEO environment.

In general, the mechanical properties of the six composite materials were not significantly degraded by exposure to the simulated LEO environment. However, most of the materials showed significant amounts of microcracking after exposure. The single-phase toughened epoxy composite T300/BP907 did not suffer microcracking after exposure to the simulated LEO environment. Therefore, if the criteria for choosing a material for use in space are that it have the smallest reduction in mechanical properties and the lowest microcrack density after exposure to a simulated environment, T300/BP907 is the best suited of the six materials studied to be used in LEO applications. With the same criteria, AS4/PEEK is the best suited of the six materials studied for use in GEO applications.

Conclusions

Six commercially available graphite-reinforced composite materials with both thermoset and thermoplastic resins were evaluated to determine the effects of 500 thermal cycles (simulated low-Earth-orbit (LEO) environment) and the effects of electron radiation followed by 500 thermal cycles (simulated geosynchronous-orbit (GEO) environment) on the glass transition temperature, microcrack density, and mechanical properties at both room temperature and −250°F. The following conclusions are drawn from this study:

1. Significant microcrack damage was found in four of the six material systems after exposure to 500 thermal cycles. However, two of the material systems, a 350°F-cure single-phase toughened epoxy system (T300/BP907) and a semicrystalline thermoplastic (AS4/PEEK) did not exhibit any significant microcrack damage after 500 thermal cycles.
2. Thermal cycling of the irradiated composite materials resulted in significant microcrack damage in all the materials except a semicrystalline thermoplastic (AS4/PEEK).
3. On the whole, the simulated LEO thermal cycling exposure did not significantly affect the mechanical properties of the materials examined in this study.
4. The simulated GEO exposure noticeably affected the mechanical properties of the materials. In the case of the two toughened epoxy systems (T300/BP907 and T300/CE339), the mechanical properties were substantially degraded.
5. No one class of materials (thermoset versus thermoplastic, toughened versus nontoughened, or amorphous versus semicrystalline) outperformed the other in terms of space durability. This study clearly indicates that accurate projections concerning space durability of a particular material cannot be made based on information on the space durability of another material in the same broad materials category.
6. Composite materials which are proven suitable for LEO applications may not have the required durability for long-term GEO applications. Hence, the "best" material for a specific space application will strongly depend on the specific orbital environment.

NASA Langley Research Center
Hampton, VA 23665-5225
February 13, 1989

References

1. Tenney, D. R.; Sykes, G. F.; and Bowles, D. E.: Composite Materials for Space Structures. *Third European Symposium on Spacecraft Materials in Space Environment*, ESA-SP-232, 1985, pp. 9–21.
2. Gounder, R. N.: Advanced Composite Antenna Reflectors for Communications Satellites. *SAMPE J.*, vol. 19, no. 3, May/June 1983, pp. 11–14.
3. Tompkins, Stephen S.; and Williams, Sharon L.: Effects of Thermal Cycling on Mechanical Properties of Graphite Polyimide. *J. Spacecr. & Rockets*, vol. 21, no. 3, May-June 1984, pp. 274–280.
4. Wolff, Ernest G.: Dimensional Stability of Carbon Fiber Reinforced Plastic Tubes. *SAMPE Q.*, vol. 16, no. 1, Oct. 1984, pp. 26–33.
5. Sykes, George F.; and Slemp, Wayne S.: Space Radiation Effects on an Elastomer-Toughened Epoxy-Graphite Composite. *Advancing Technology in Materials and Processes—30th National SAMPE Symposium and Exhibition*, Volume 30, Soc. for the Advancement of Material and Process Engineering, c.1985, pp. 1356–1374.

6. Cohen, David; Hyer, Michael W.; and Tompkins, Stephen S.: The Effects of Thermal Cycling on Matrix Cracking and Stiffness Changes in Composite Tubes. *Hi-Tech Review 1984—16th National SAMPE Technical Conference*, Volume 16, Soc. for the Advancement of Material and Process Engineering, c.1984, pp. 577–588.
7. Milkovich, Scott M.; Herakovich, Carl T.; and Sykes, George F.: Space Radiation Effects on the Thermo-Mechanical Behavior of Graphite-Epoxy Composites. *J. Compos. Mater.*, vol. 20, no. 6, Nov. 1986, pp. 579–593.
8. Kong, Eric S. W.: Influence of Physical Aging on the Time-Dependent Properties of Network Epoxies and Epoxy-Matrix Composites. *Epoxy Resin Chemistry II*, Ronald S. Bauer, ed., ACS Symposium Series 221, American Chemical Soc., 1983, pp. 171–191.
9. Santos, Beatrice; and Sykes, George F.: Radiation Effects on Four Polysulfone Films. *Technology Transfer—13th National SAMPE Technical Conference*, Volume 13, Soc. for the Advancement of Material and Process Engineering, c.1981, pp. 256–269.
10. Funk, Joan G.; and Sykes, George F., Jr.: Space Radiation Effects on Poly[Aryl-Ether-Ketone] Thin Films and Composites. *SAMPE Q.*, vol. 19, no. 3, Apr. 1988, pp. 19–26.

Table I. Summary of Materials

Composite fiber[a]/matrix	Prepreg source	Processing	Matrix description
T300/934	Fiberite Corp.	LaRC[b]	350°F-cure epoxy
T300/BP907	American Cyanamid Co.	LaRC[b]	350°F-cure single-phase toughened epoxy
T300/CE339	Ferro Corp.	LaRC[b]	250°F-cure two-phase elastomer-toughened epoxy
C6000/P1700	Union Carbide Corp.	LaRC[b]	Polysulfone, amorphous thermoplastic
AS4/PPS	Phillips Petroleum	Phillips Petroleum	Polyphenylene sulfide, semicrystalline thermoplastic
AS4/PEEK	ICI Americas Inc.	ICI	Polyetherether ketone, semicrystalline thermoplastic

[a]T300, C6000, and AS4 are polyacrylonitrile-based graphite fibers.
[b]Processed at the Langley Research Center using manufacturers' recommended cure cycle.

Table II. Physical Characteristics of Materials Tested

Composite fiber/matrix	Fiber volume fraction, percent	Volatile content, percent	Density, lb/in^3
T300/934	56.8	0.4	0.0571
T300/BP907	54.8	.3	.0549
T300/CE339	53.8	.6	.0556
C6000/P1700	55.2	.1	.0560
AS4/PPS	52.1	.1	.0560
AS4/PEEK	Did not digest	.1	.0571

Table III. Microcrack Density of Six Quasi-Isotropic Graphite Fiber Composites

Material	Microcrack density, cracks/in., for—		
	Baseline specimens	Thermal cycled specimens	Irradiated[a] and thermal cycled specimens
T300/934	0	[b]18	[b]43
T300/BP907	0	[b]0	[b] >100
T300/CE339	0	[c]20	[c]64
C6000/P1700	13	[b]53	[b]61
AS4/PPS	0	[c]48	[c]56
AS4/PEEK	0	[b]3	[b]13

[a]1×10^{10} rads electron radiation.
[b]500 thermal cycles: −250°F to 200°F.
[c]500 thermal cycles: −250°F to 150°F.

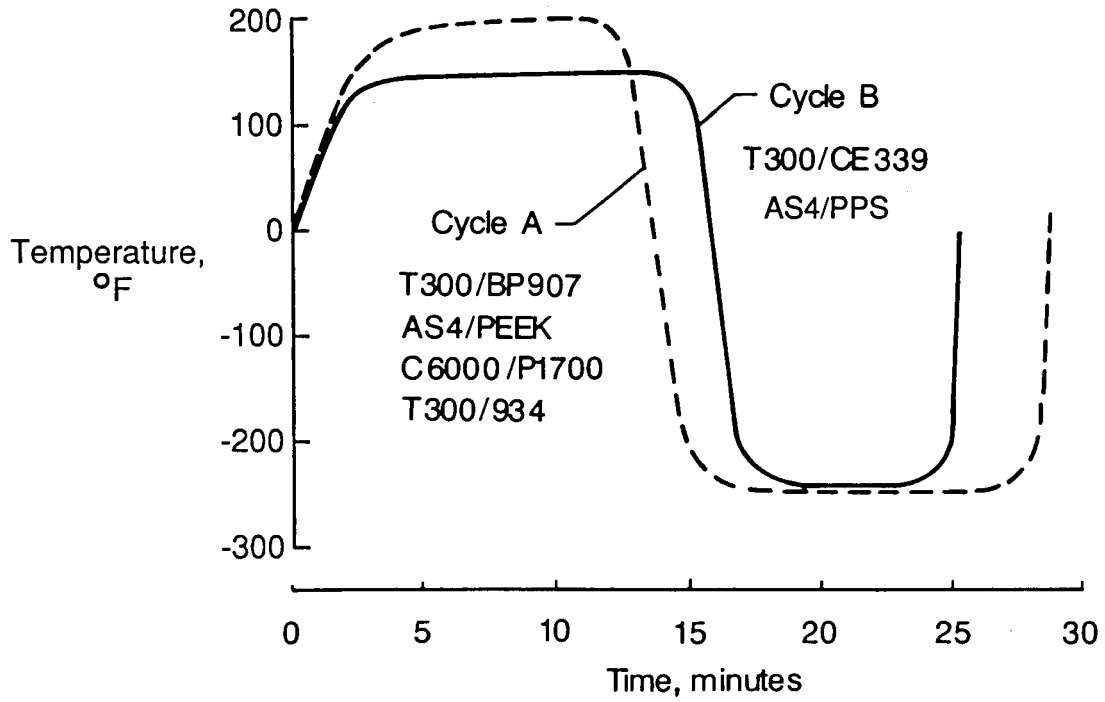

Figure 1. Typical thermal cycle used in present study. Cycles performed in nitrogen at atmospheric pressure.

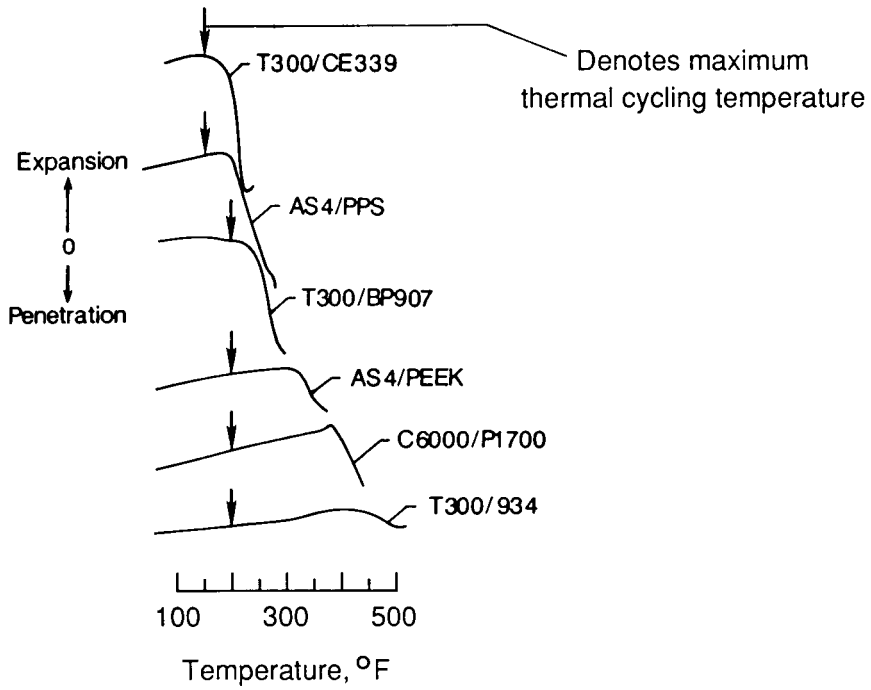

Figure 2. Thermomechanical analysis data and maximum thermal cycling temperature of six commercially available graphite-fiber composites. Specimen was heated at rate of 9°F/min in a nitrogen atmosphere.

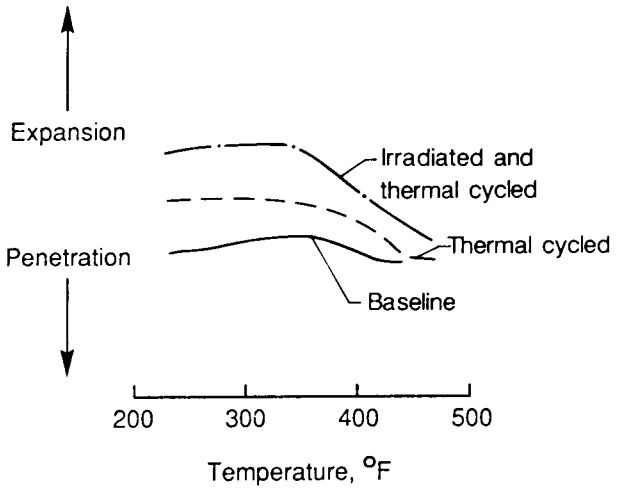

Glass transition temperature of T300/934, °F

Baseline	Thermal cycled[1]	Irradiated[2] and thermal cycled[1]
360	360	338

[1] 500 thermal cycles: -250°F to 200°F
[2] 1×10^{10} rads electron radiation

Figure 3. Thermomechanical analysis data and glass transition temperature of T300/934.

Microcrack density, cracks/in.

Baseline	Thermal cycled[1]	Irradiated[2] and thermal cycled[1]
0	18	43

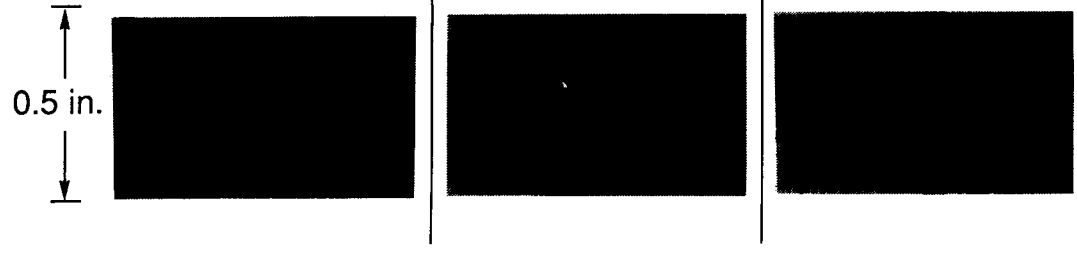

[1] 500 thermal cycles: - 250°F to 200°F
[2] 1×10^{10} rads electron radiation

Figure 4. Microcrack density in T300/934.

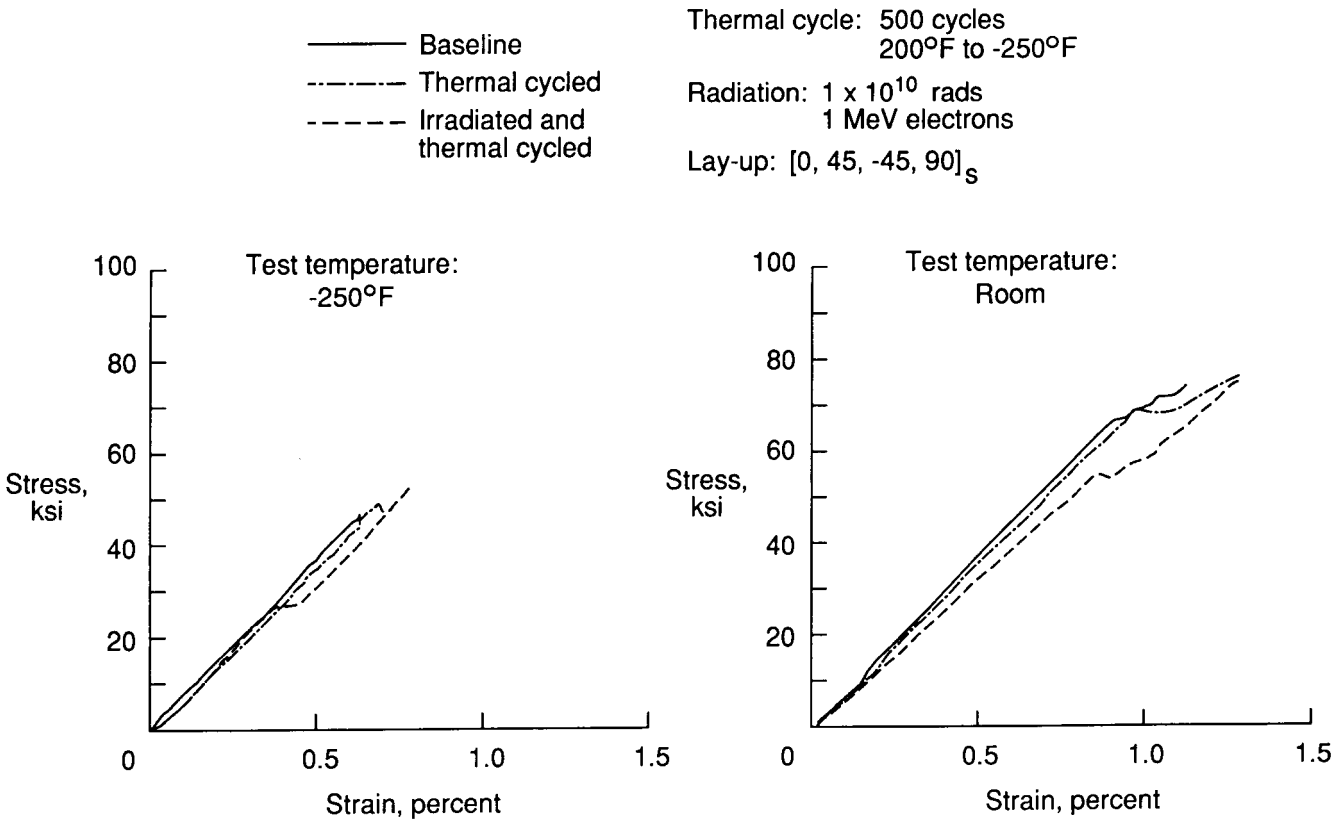

Figure 5. Typical stress-strain curves of T300/934.

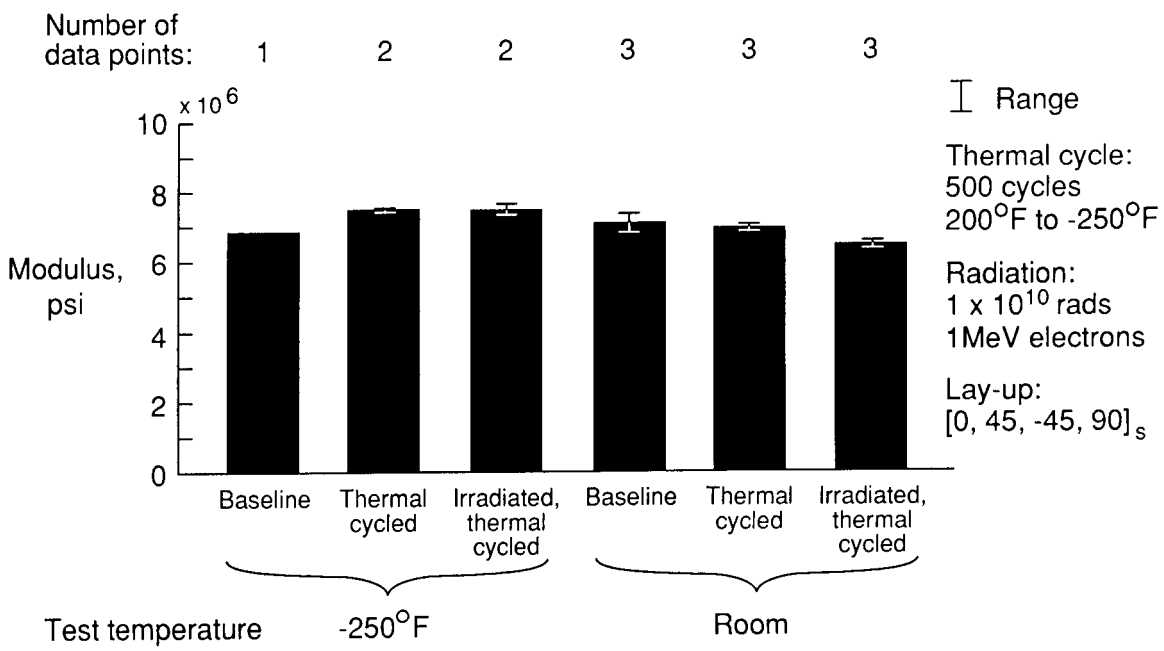

Figure 6. Modulus of T300/934.

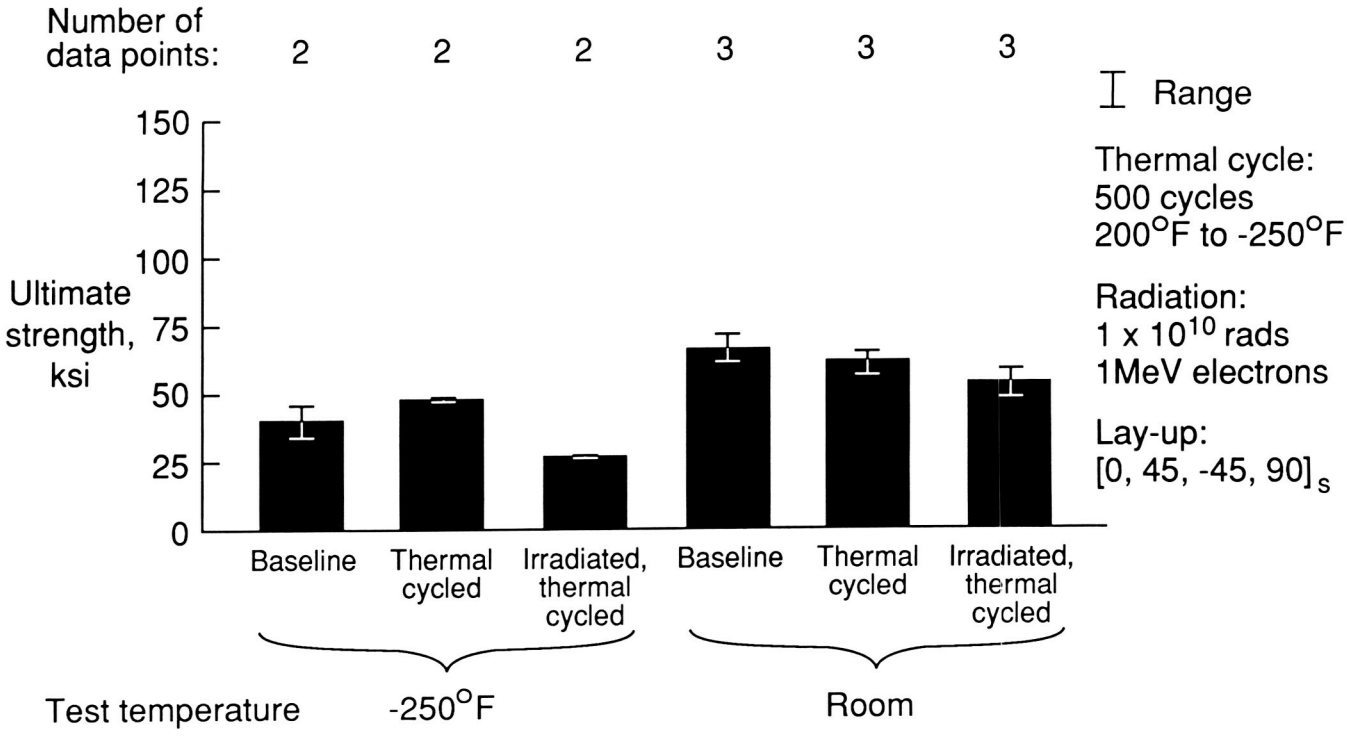

Figure 7. Ultimate strength of T300/934.

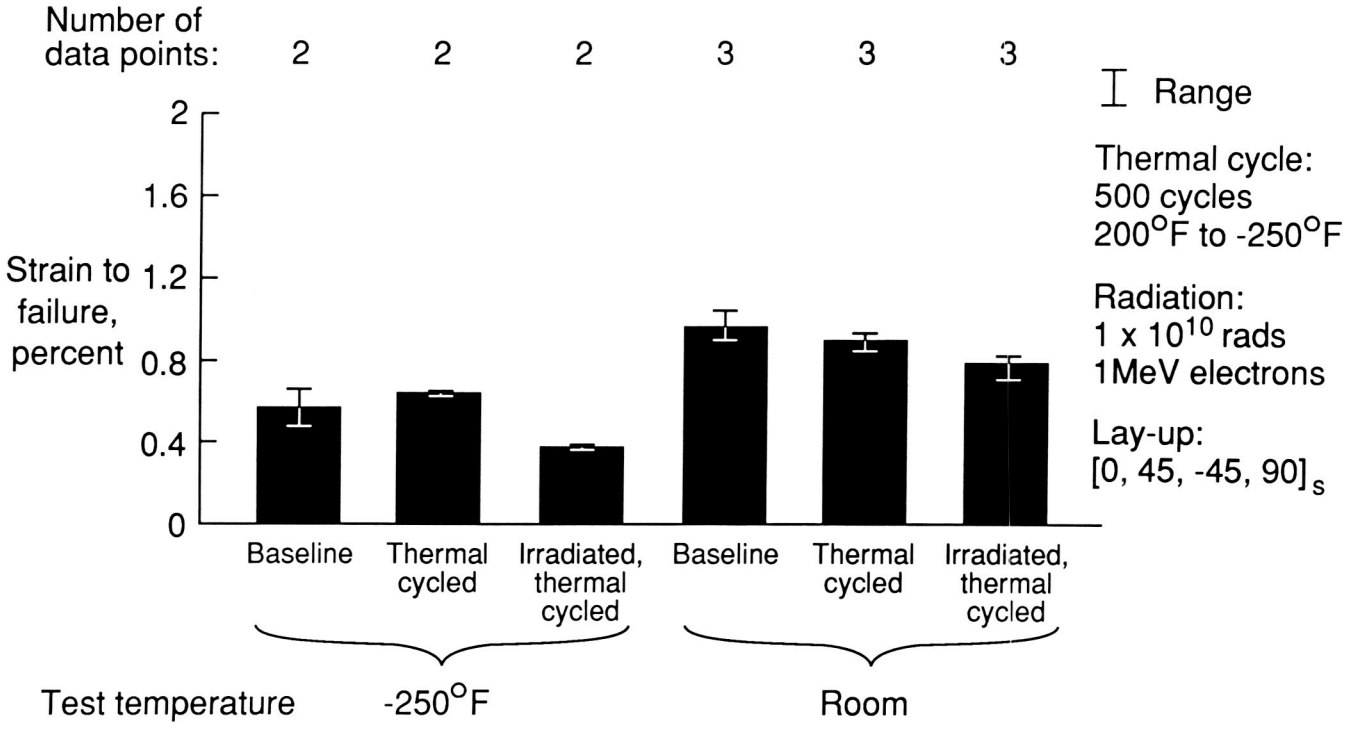

Figure 8. Failure strain of T300/934.

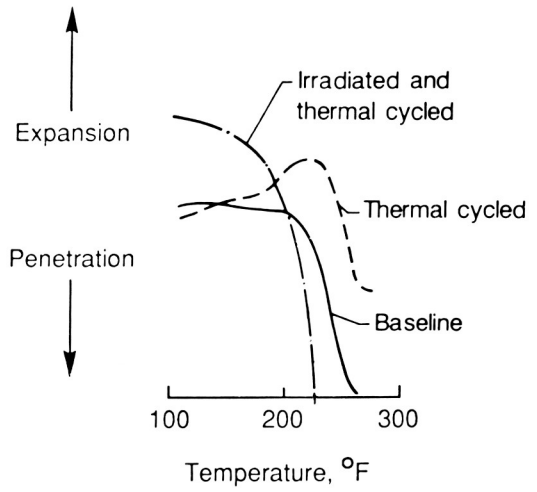

Glass transition temperature of T300/BP907, °F

Baseline	Thermal cycled [1]	Irradiated [2] and thermal cycled [1]
216	230	207

[1] 500 thermal cycles: -250°F to 200°F
[2] 1 x 10^{10} rads electron radiation

Figure 9. Thermomechanical analysis data and glass transition temperature of T300/BP907.

Microcrack density, cracks/in.

Baseline	Thermal cycled [1]	Irradiated [2] and thermal cycled [1]
0	0	>100

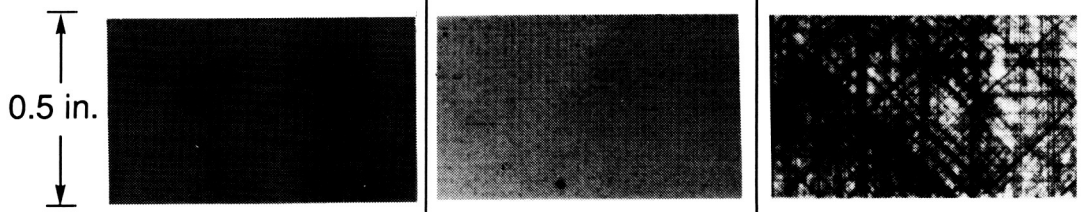

Cracking and delamination extensive

[1] 500 thermal cycles: - 250°F to 200°F
[2] 1 x 10^{10} rads electron radiation

Figure 10. Microcrack density in T300/BP907.

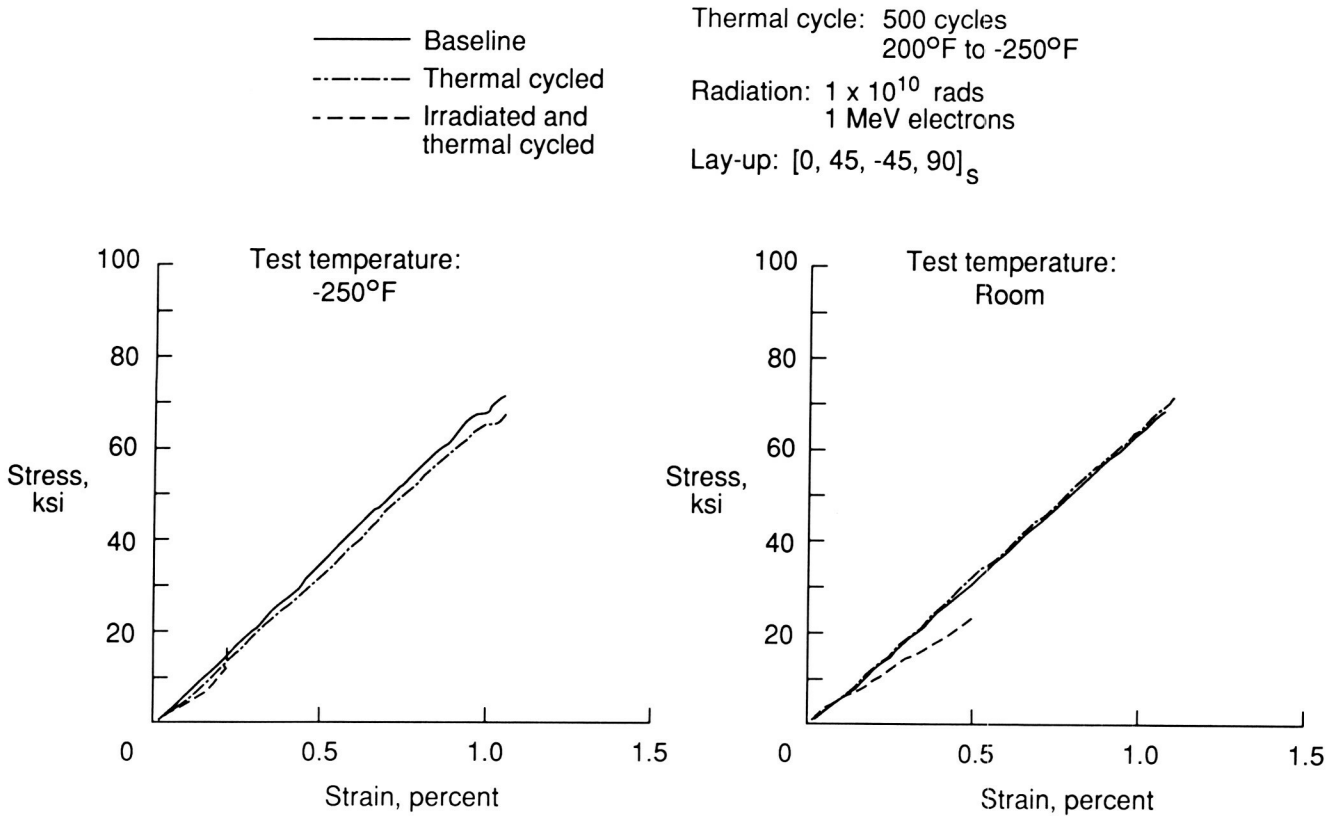

Figure 11. Typical stress-strain curves of T300/BP907.

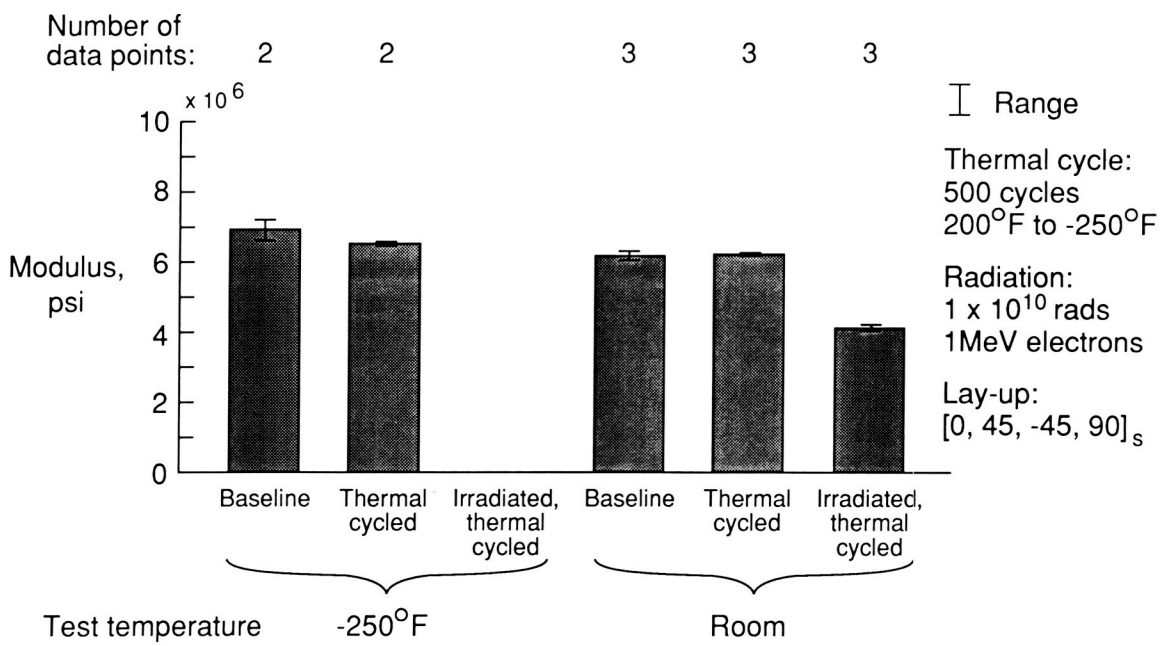

Figure 12. Modulus of T300/BP907.

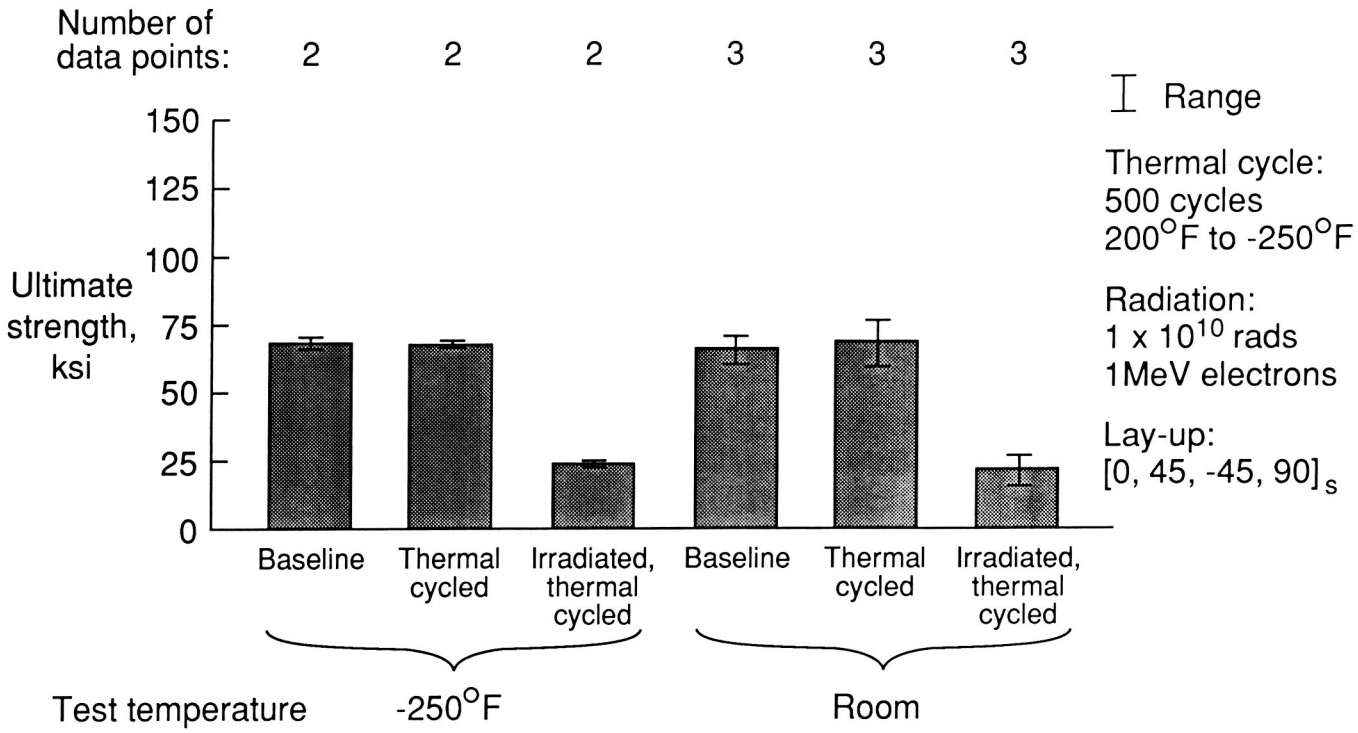

Figure 13. Ultimate strength of T300/BP907.

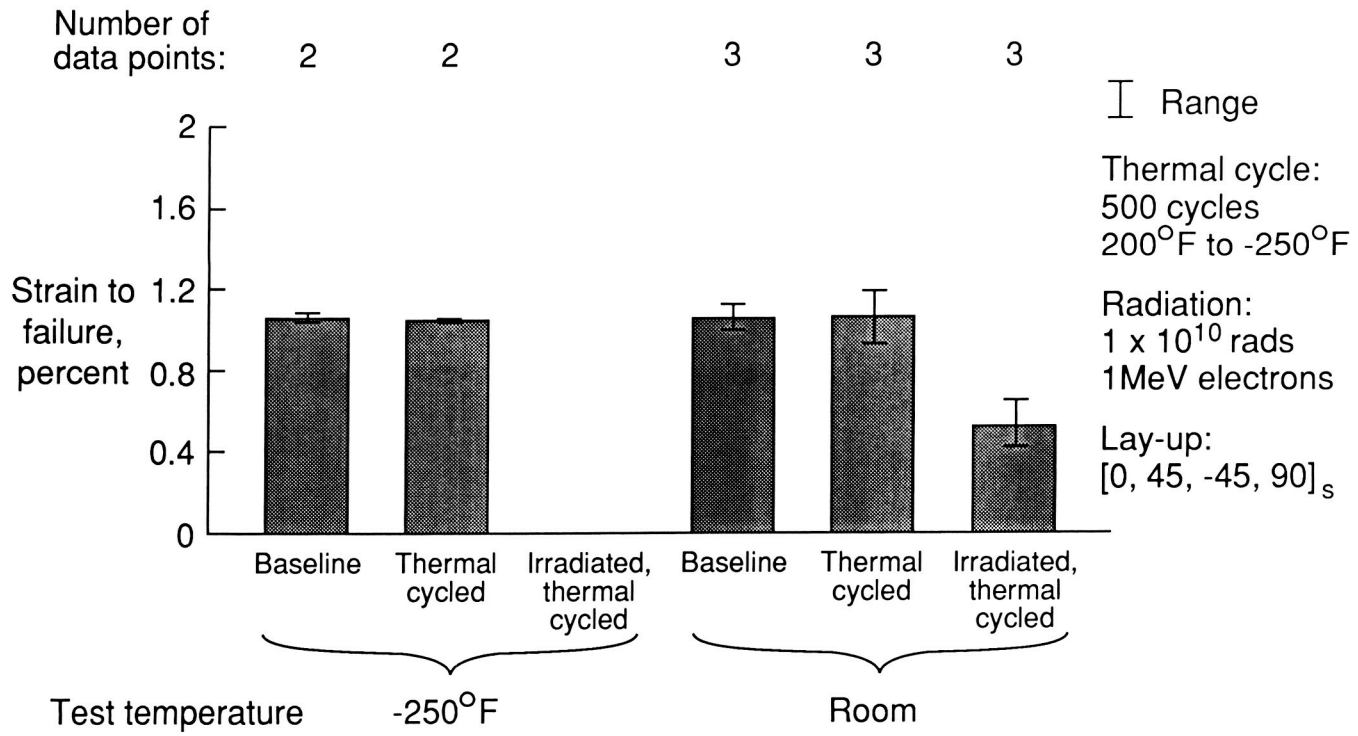

Figure 14. Failure strain of T300/BP907.

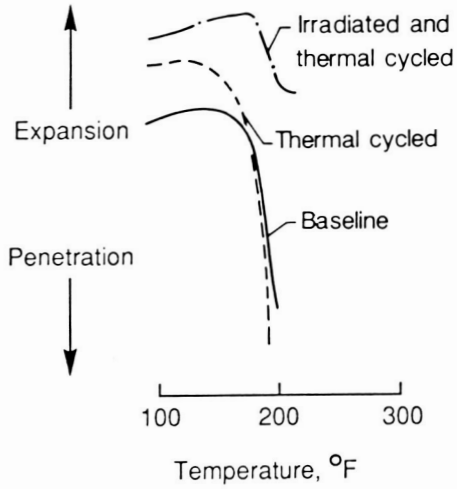

Glass transition temperature of T300/CE339, °F

Baseline	Thermal cycled[1]	Irradiated[2] and thermal cycled[1]
176	173	176

[1] 500 thermal cycles: -250°F to 150°F
[2] 1 x 10^{10} rads electron radiation

Figure 15. Thermomechanical analysis data and glass transition temperature of T300/CE339.

Microcrack density, cracks/in.

Baseline	Thermal cycled[1]	Irradiated[2] and thermal cycled[1]
0	20	64

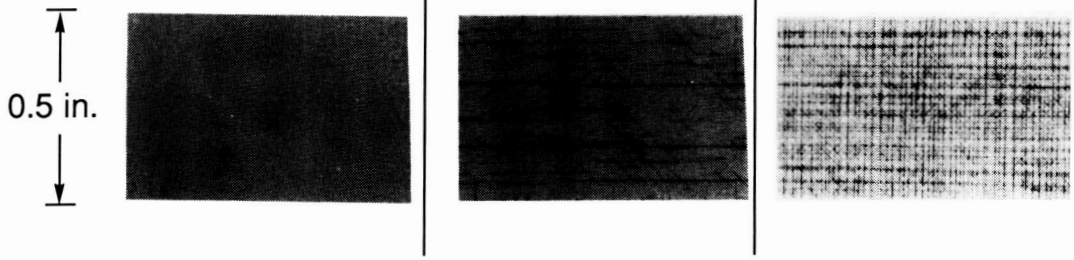

[1] 500 thermal cycles: - 250°F to 150°F
[2] 1 x 10^{10} rads electron radiation

Figure 16. Microcrack density in T300/CE339.

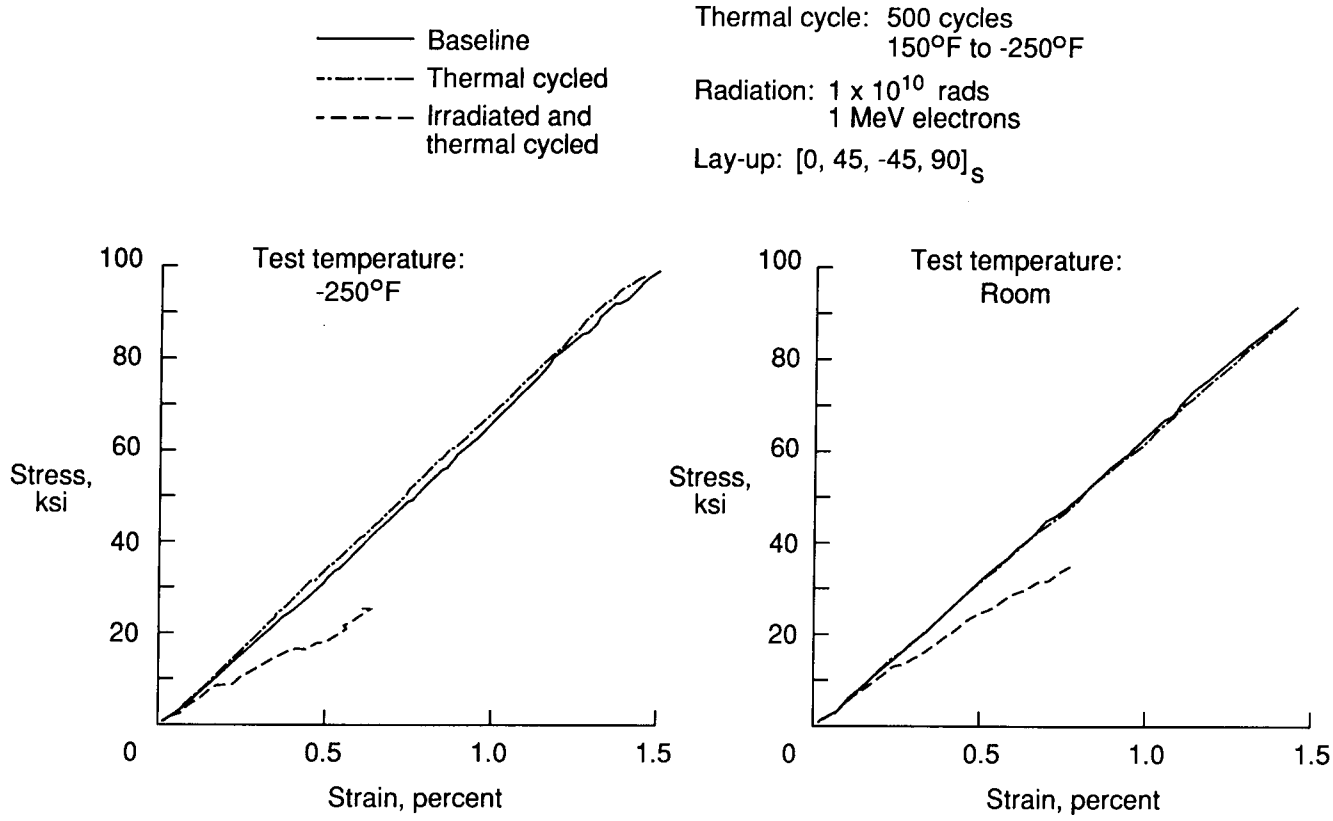

Figure 17. Typical stress-strain curves of T300/CE339.

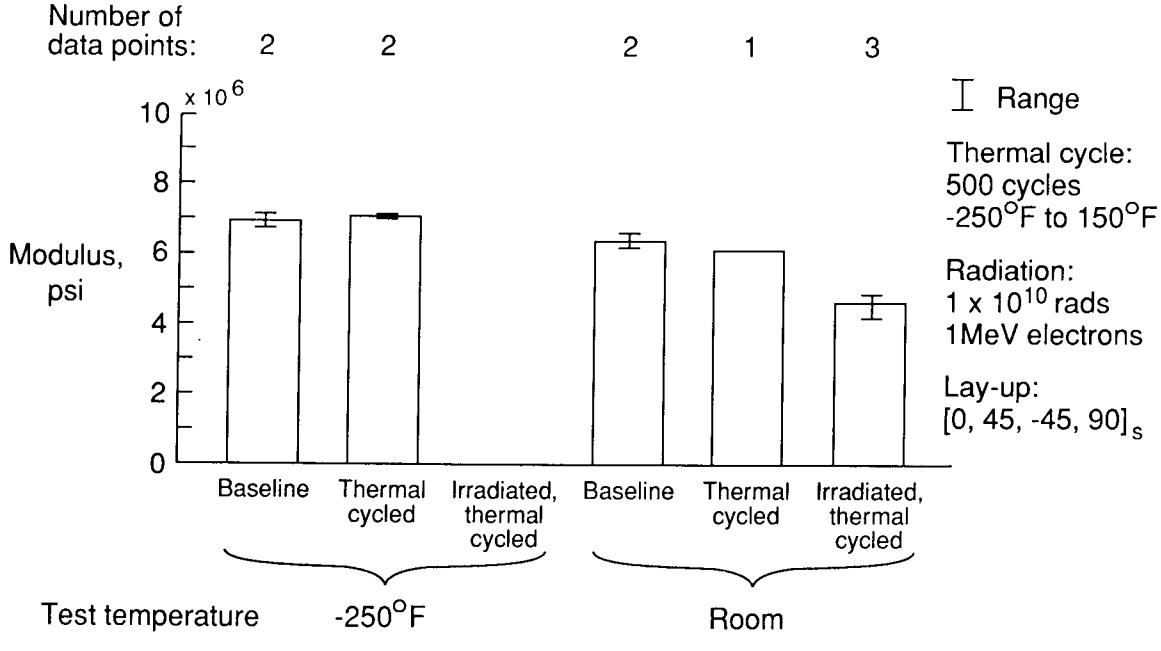

Figure 18. Modulus of T300/CE339.

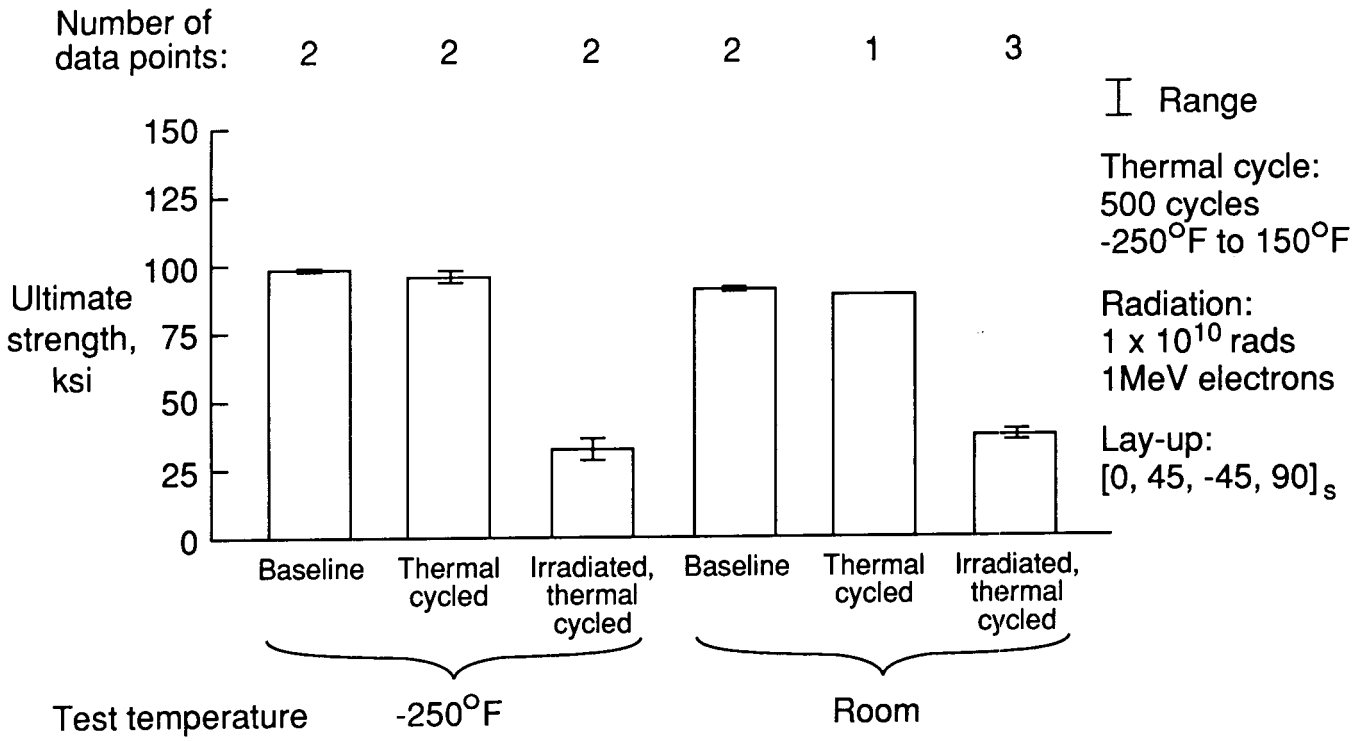

Figure 19. Ultimate strength of T300/CE339.

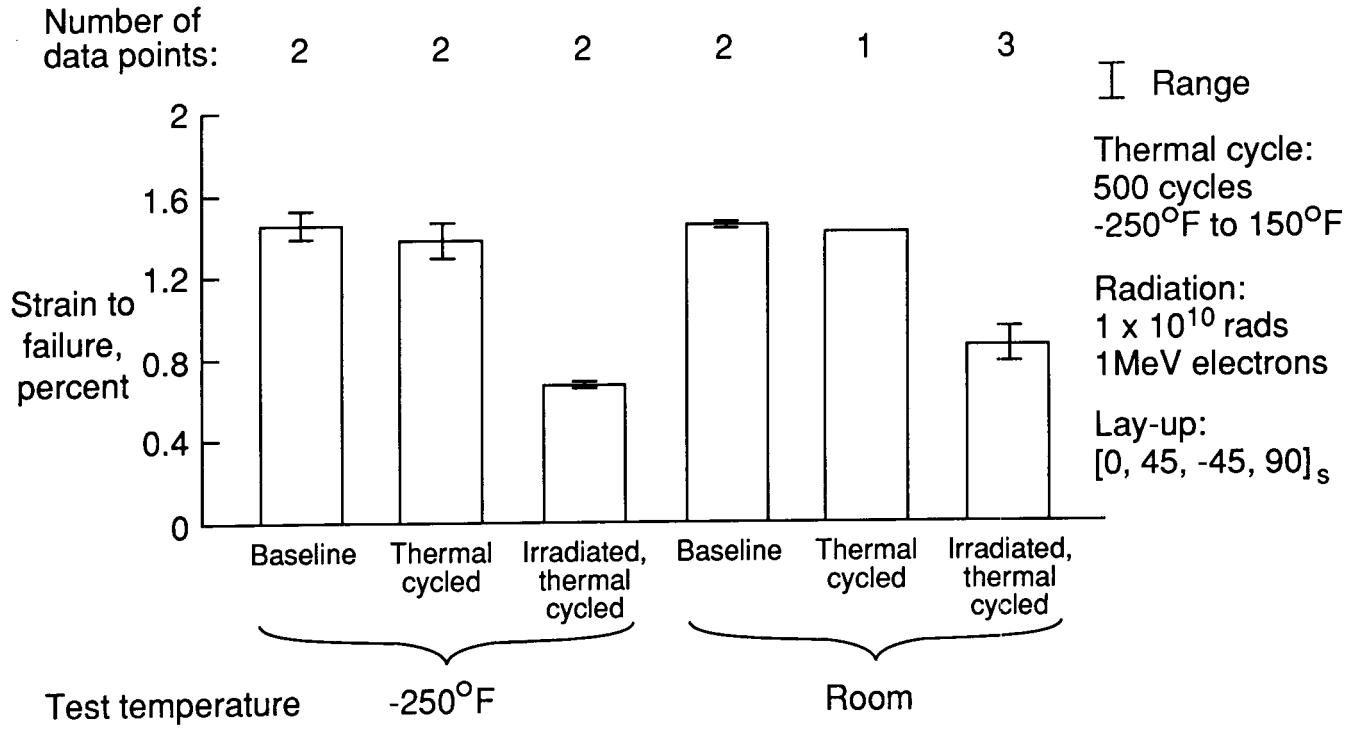

Figure 20. Failure strain of T300/CE339.

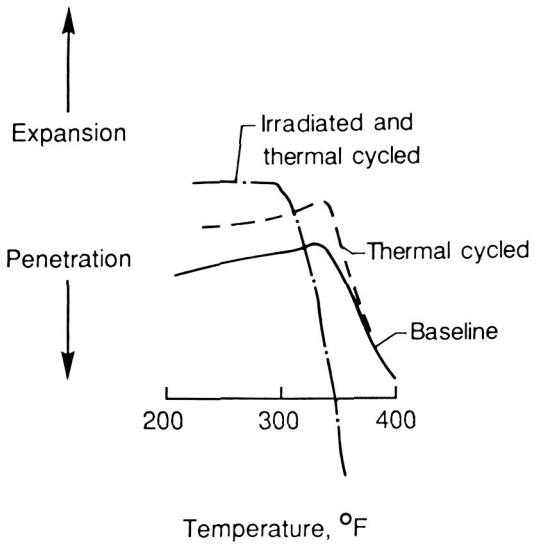

Glass transition temperature of C6000/P1700, °F

Baseline	Thermal cycled [1]	Irradiated [2] and thermal cycled [1]
336	334	315

[1] 500 thermal cycles: -250°F to 200°F
[2] 1 x 10^{10} rads electron radiation

Figure 21. Thermomechanical analysis data and glass transition temperature of C6000/P1700.

Microcrack density, cracks/in.

Baseline	Thermal cycled [1]	Irradiated [2] and thermal cycled [1]
13	53	61

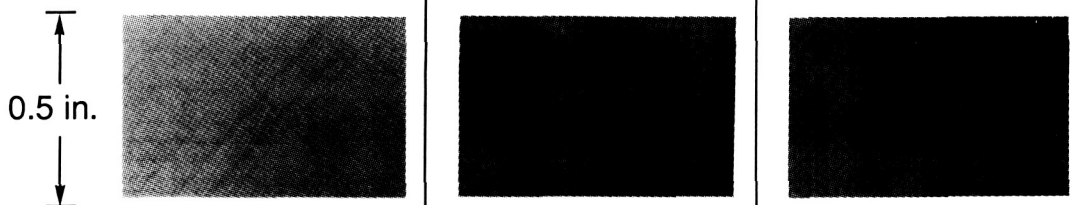

[1] 500 thermal cycles: - 250°F to 200°F
[2] 1 x 10^{10} rads electron radiation

Figure 22. Microcrack density in C6000/P1700.

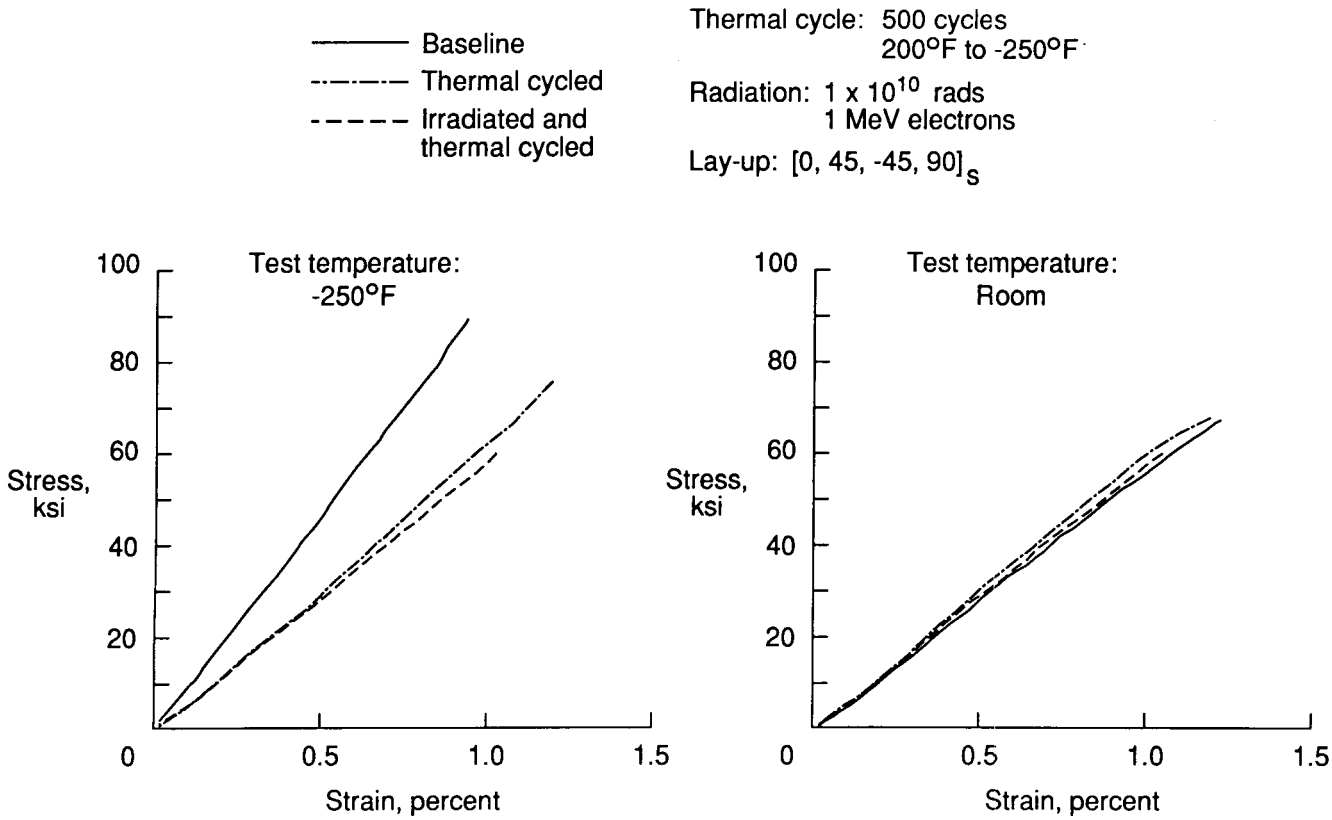

Figure 23. Typical stress-strain curves of C6000/P1700.

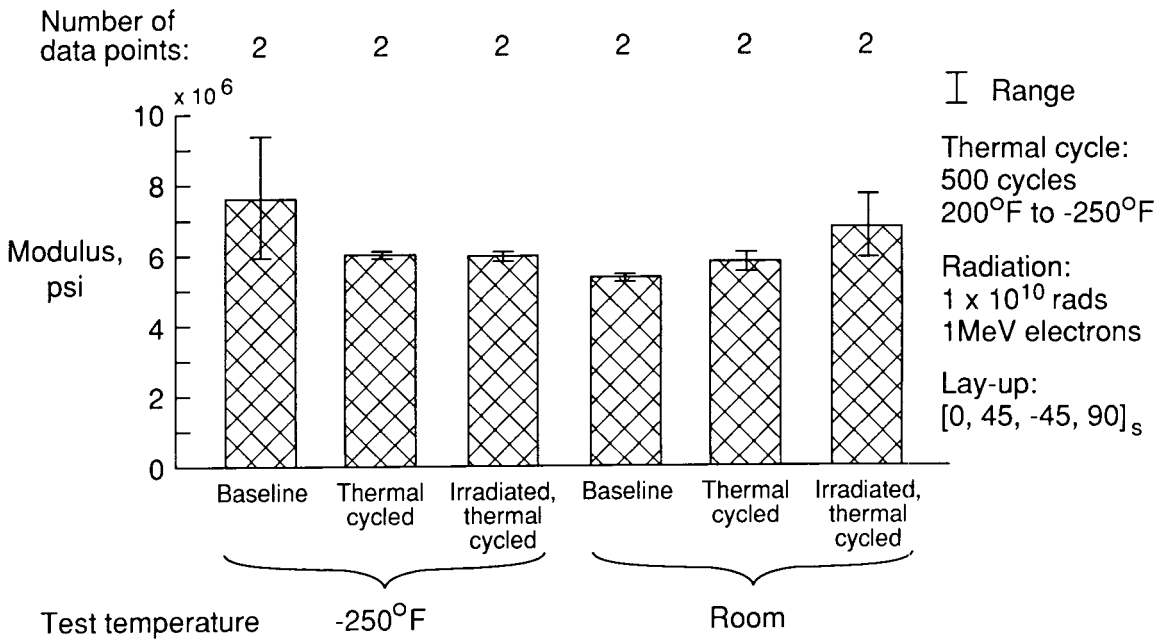

Figure 24. Modulus of C6000/P1700.

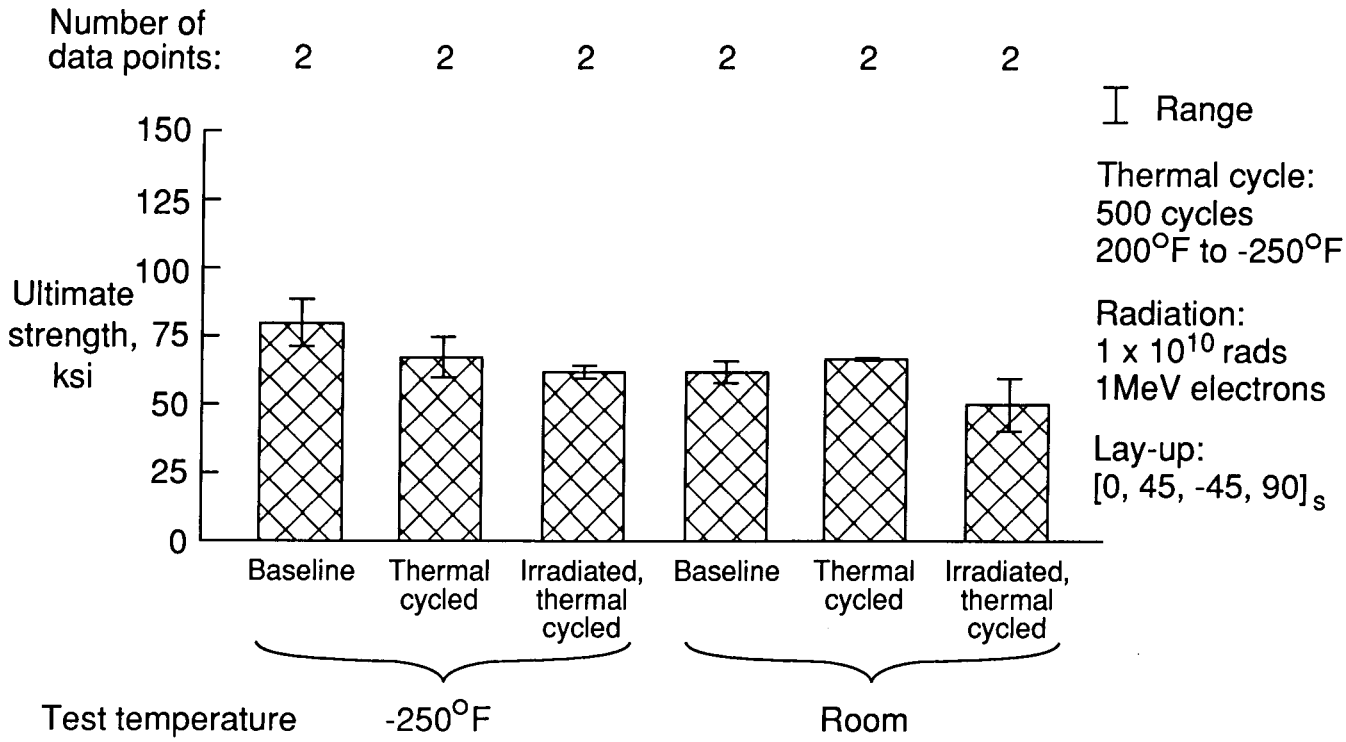

Figure 25. Ultimate strength of C6000/P1700.

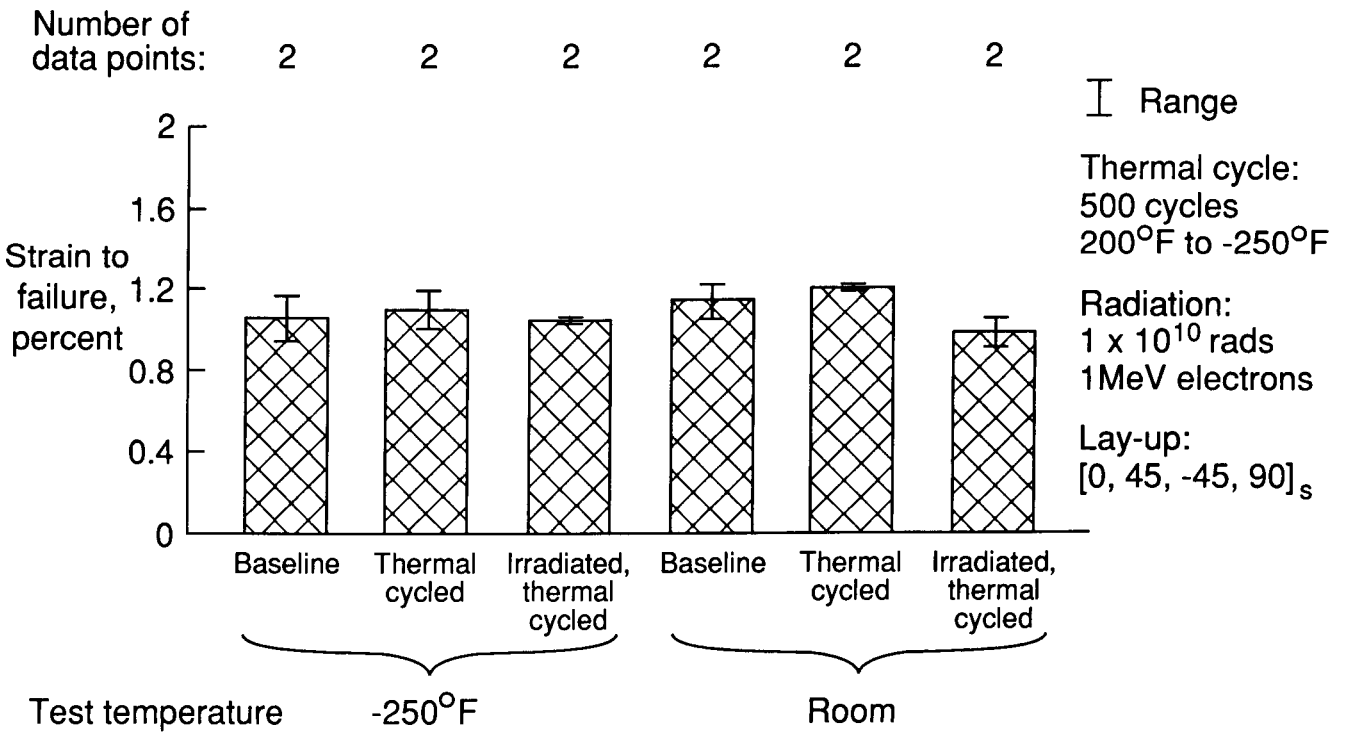

Figure 26. Failure strain of C6000/P1700.

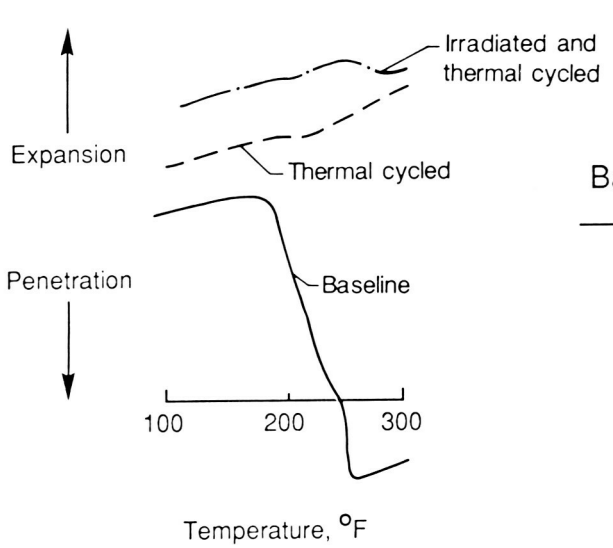

Glass transition temperature of the amorphous phase of AS4/PPS, °F

Baseline	Thermal cycled[1]	Irradiated[2] and thermal cycled[1]
180	180	185

[1] 500 thermal cycles: -250°F to 150°F
[2] 1 x 10^{10} rads electron radiation

Figure 27. Thermomechanical analysis data and glass transition temperature of AS4/PPS.

Microcrack density, cracks/in.

Baseline	Thermal cycled[1]	Irradiated[2] and thermal cycled[1]
0	48	56

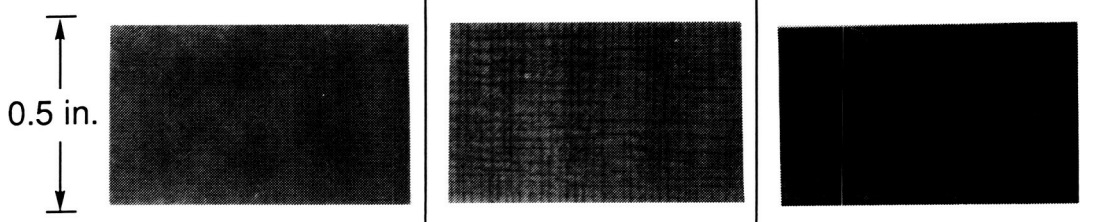

[1] 500 thermal cycles: - 250°F to 150°F
[2] 1 x 10^{10} rads electron radiation

Figure 28. Microcrack density in AS4/PPS.

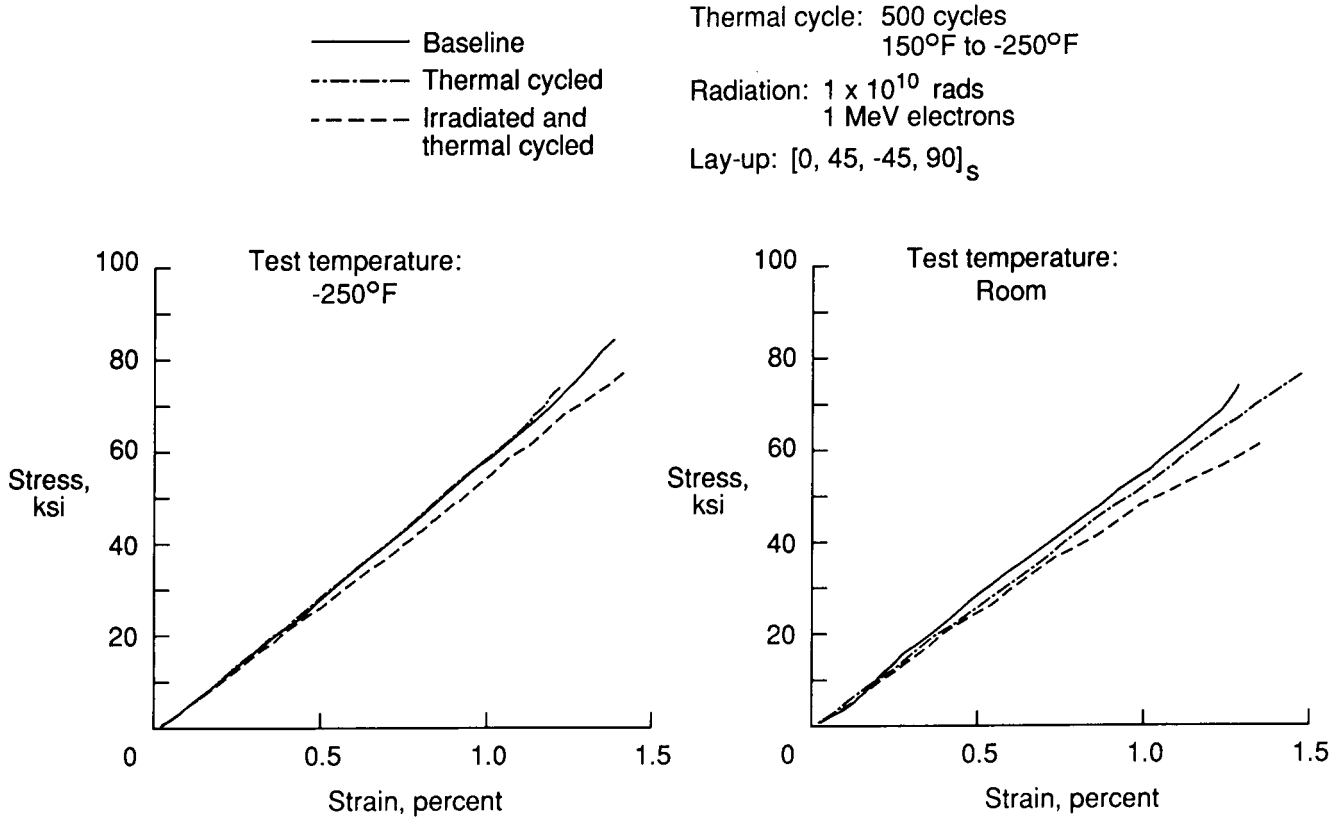

Figure 29. Typical stress-strain curves of AS4/PPS.

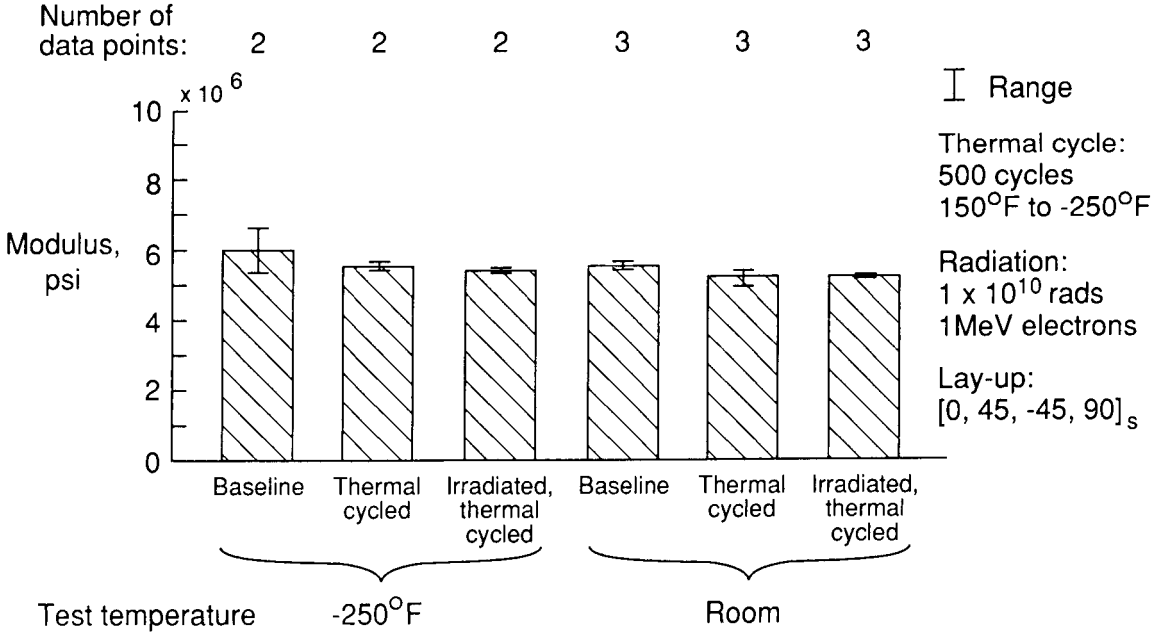

Figure 30. Modulus of AS4/PPS.

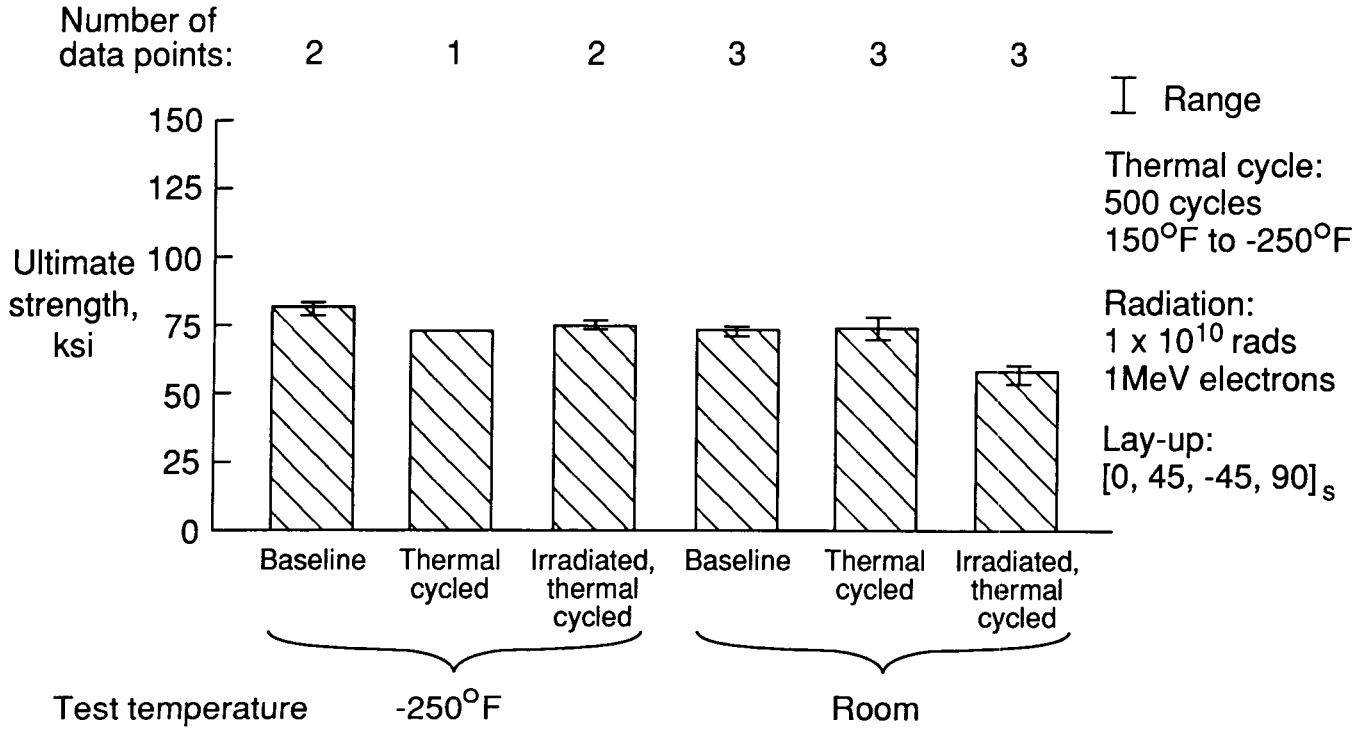

Figure 31. Ultimate strength of AS4/PPS.

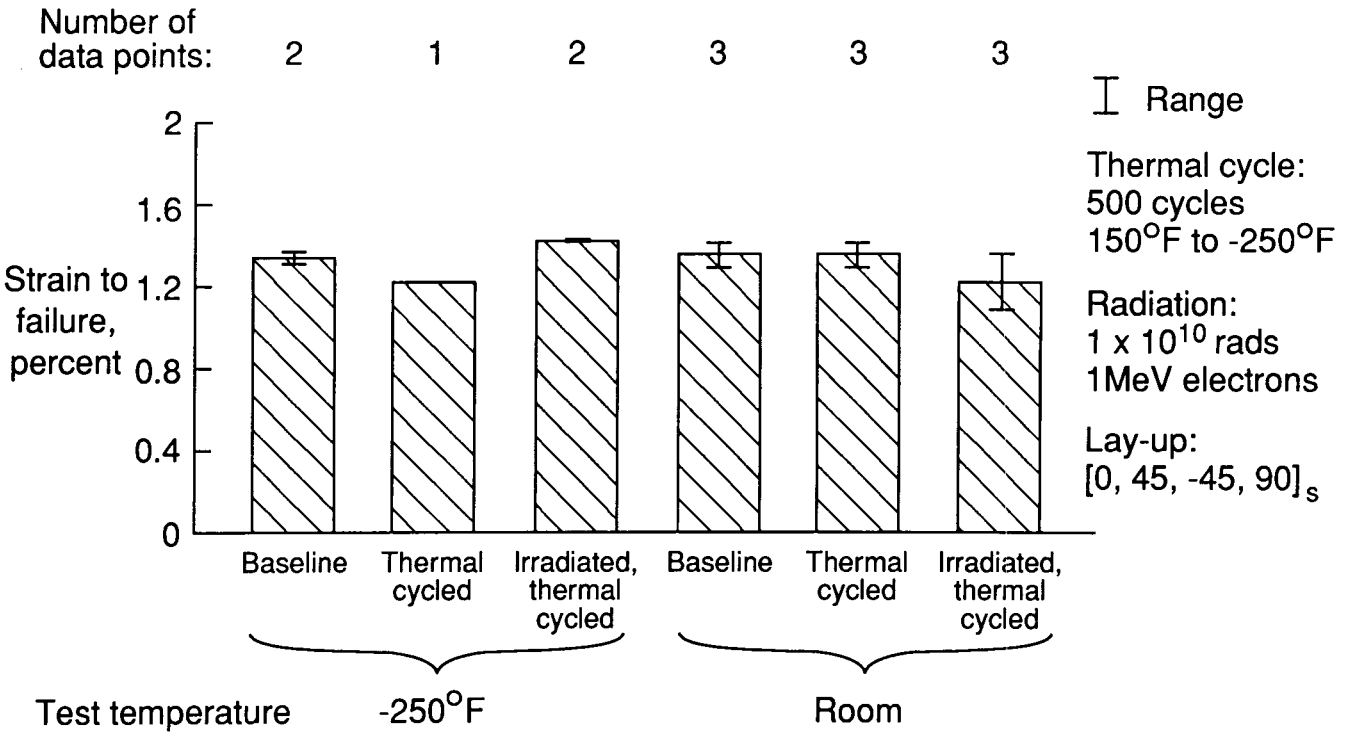

Figure 32. Failure strain of AS4/PPS.

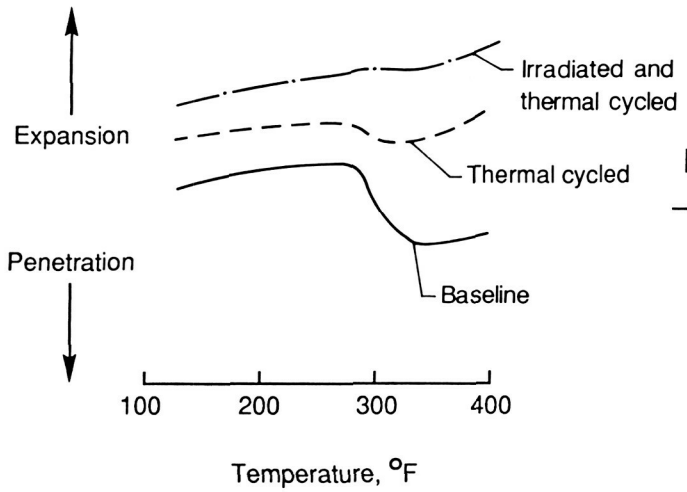

Glass transition temperature of the amorphous phase of AS4/PEEK, °F

Baseline	Thermal cycled[1]	Irradiated[2] and thermal cycled[1]
284	277	288

[1] 500 thermal cycles: -250°F to 200°F
[2] 1 x 10^{10} rads electron radiation

Figure 33. Thermomechanical analysis data and glass transition temperature of AS4/PEEK.

Microcrack density, cracks/in.

Baseline	Thermal cycled[1]	Irradiated[2] and thermal cycled[1]
0	3	13

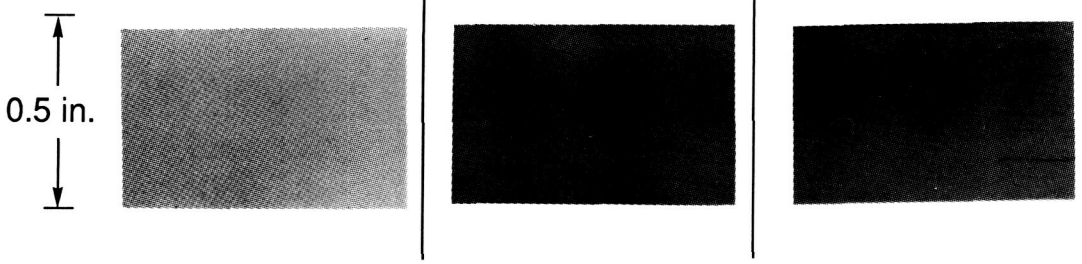

[1] 500 thermal cycles: - 250°F to 200°F
[2] 1 x 10^{10} rads electron radiation

Figure 34. Microcrack density in AS4/PEEK.

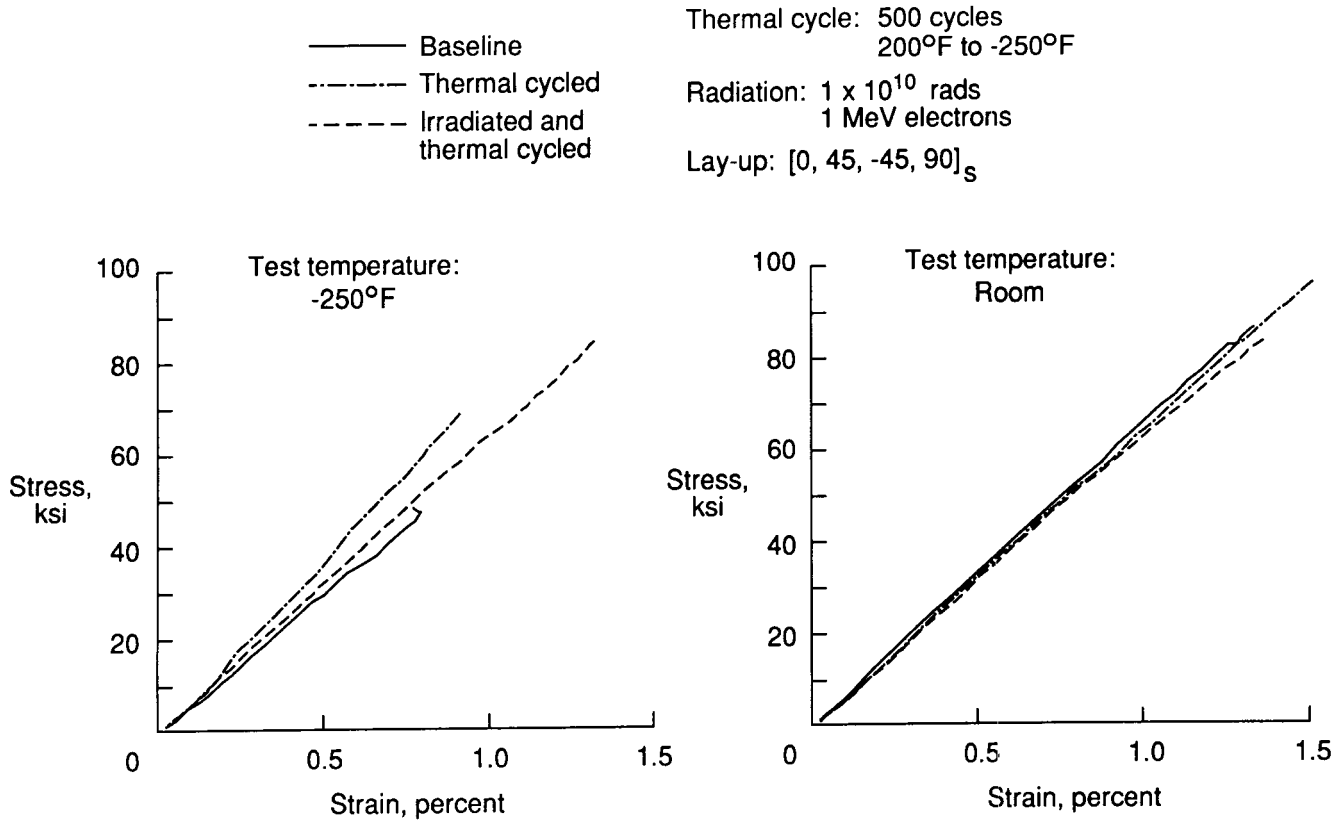

Figure 35. Typical stress-strain curves of AS4/PEEK.

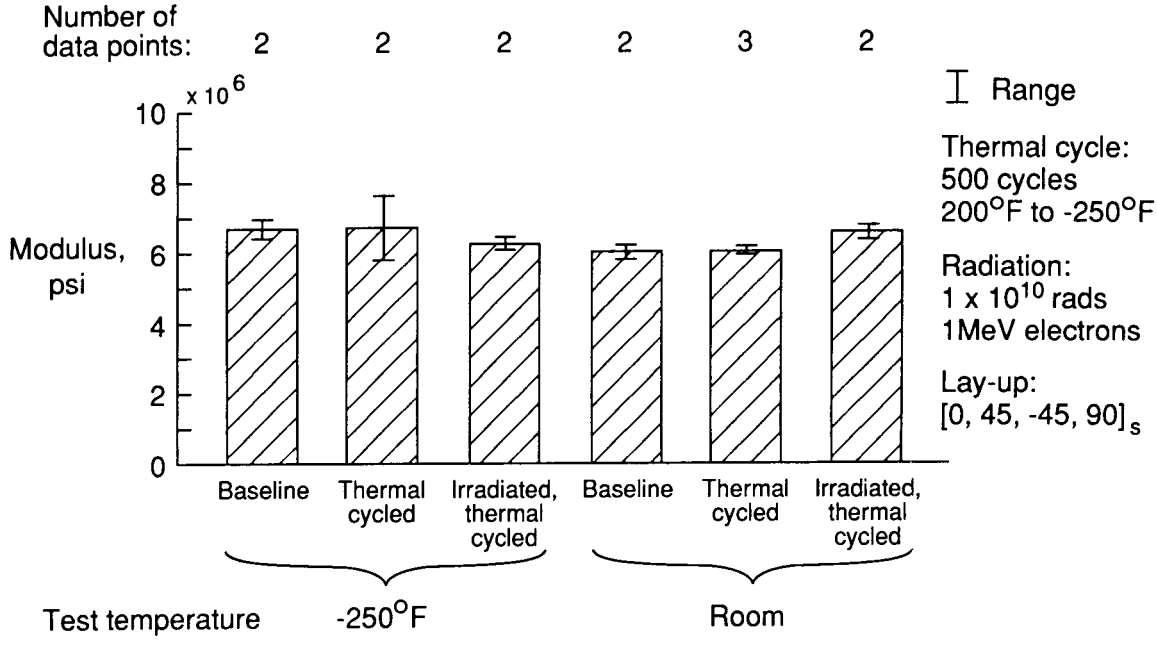

Figure 36. Modulus of AS4/PEEK.

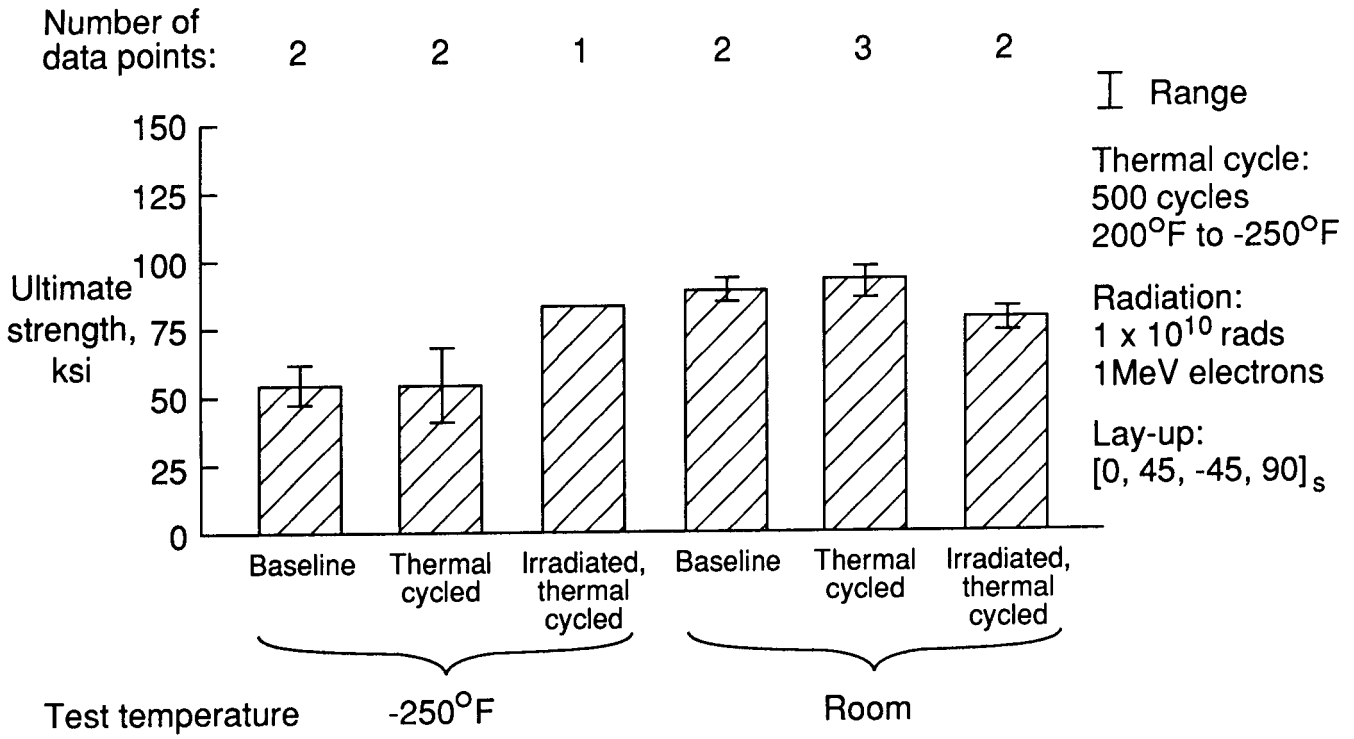

Figure 37. Ultimate strength of AS4/PEEK.

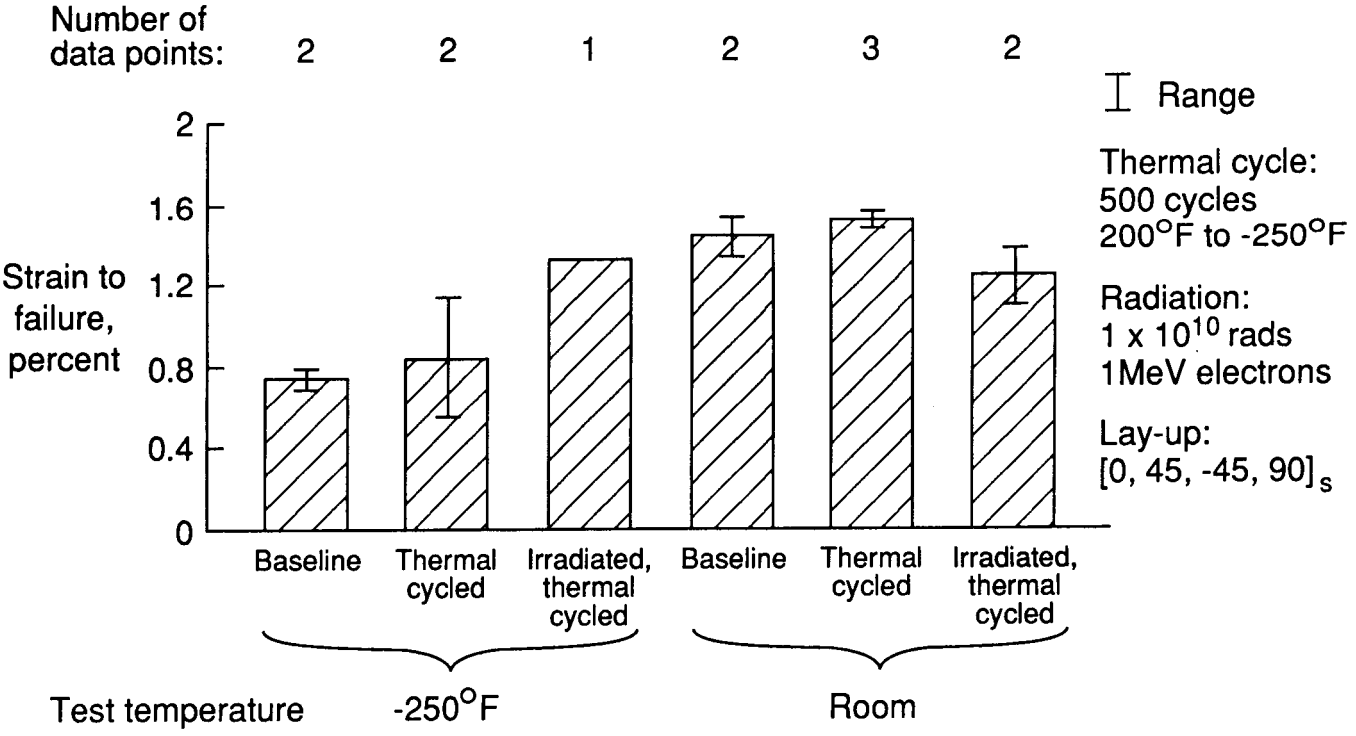

Figure 38. Failure strain of AS4/PEEK.

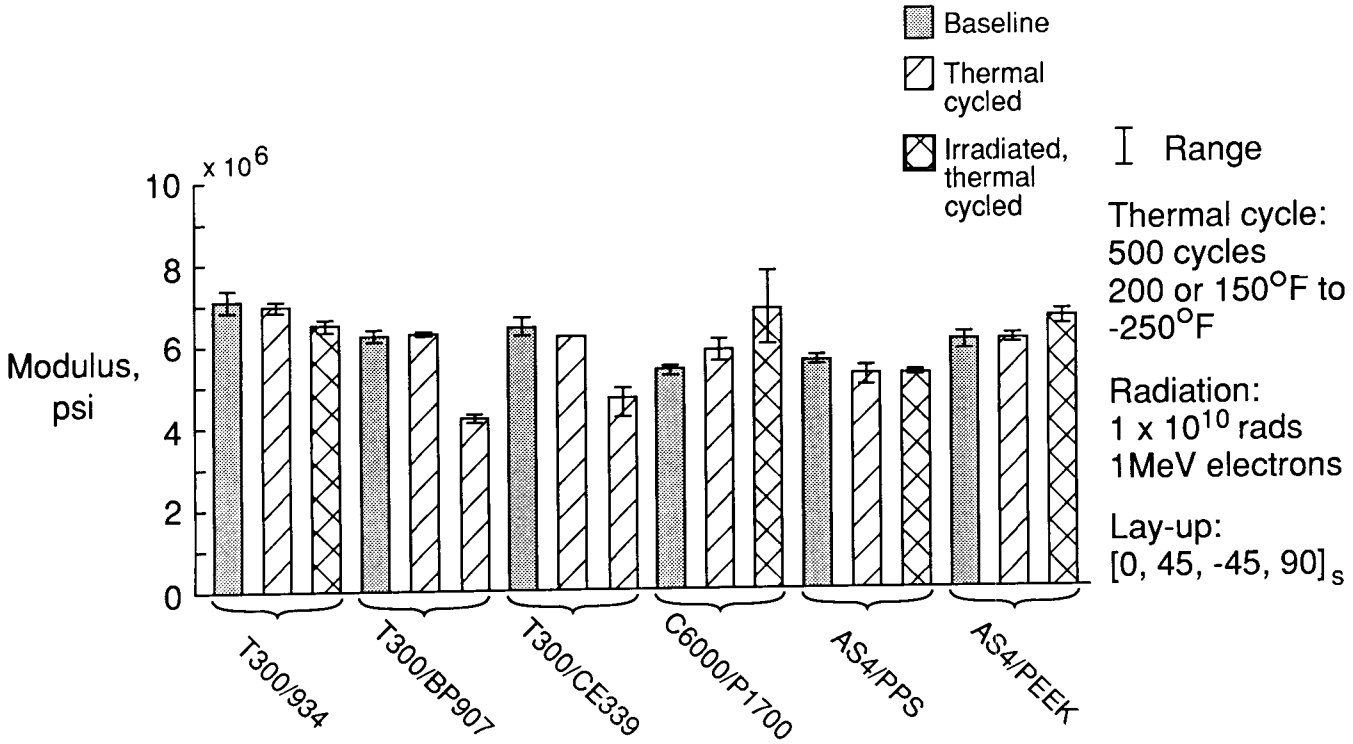

Figure 39. Modulus at room temperature of six quasi-isotropic graphite fiber composites.

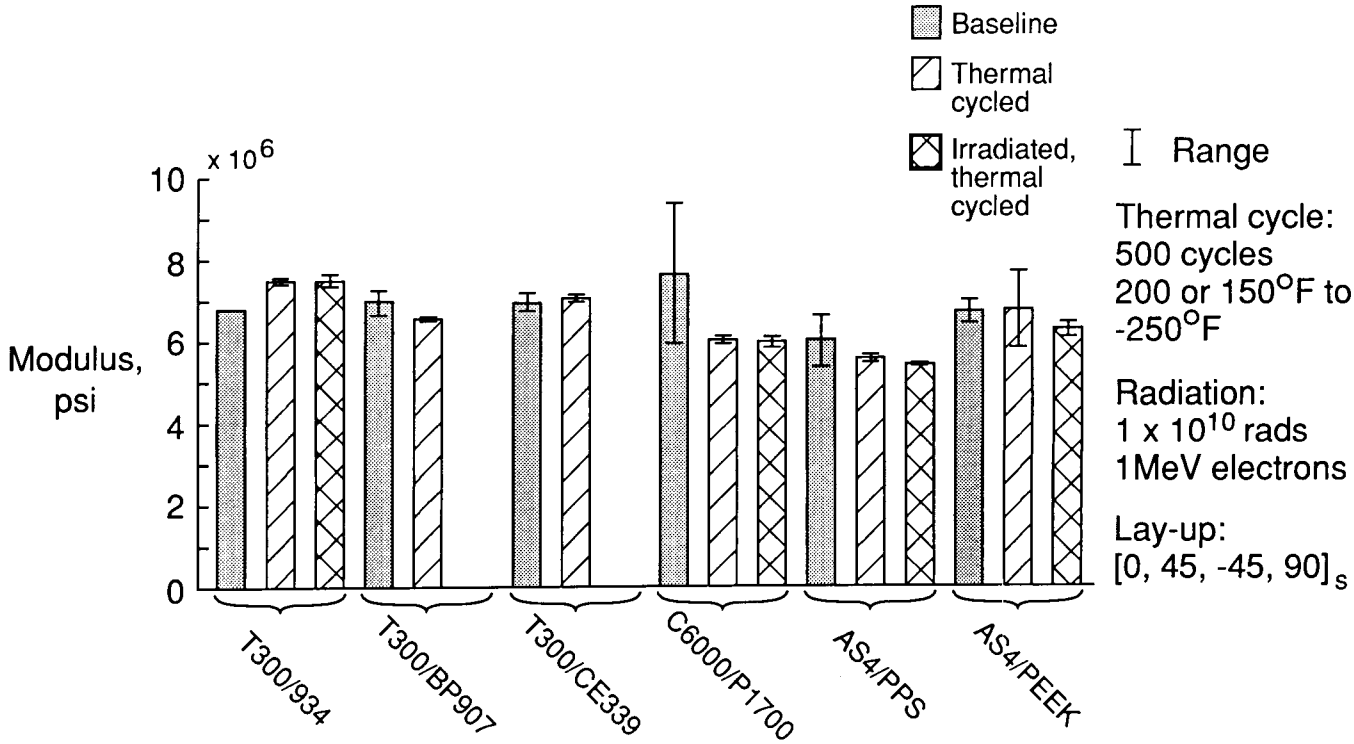

Figure 40. Modulus at −250°F of six quasi-isotropic graphite fiber composites.

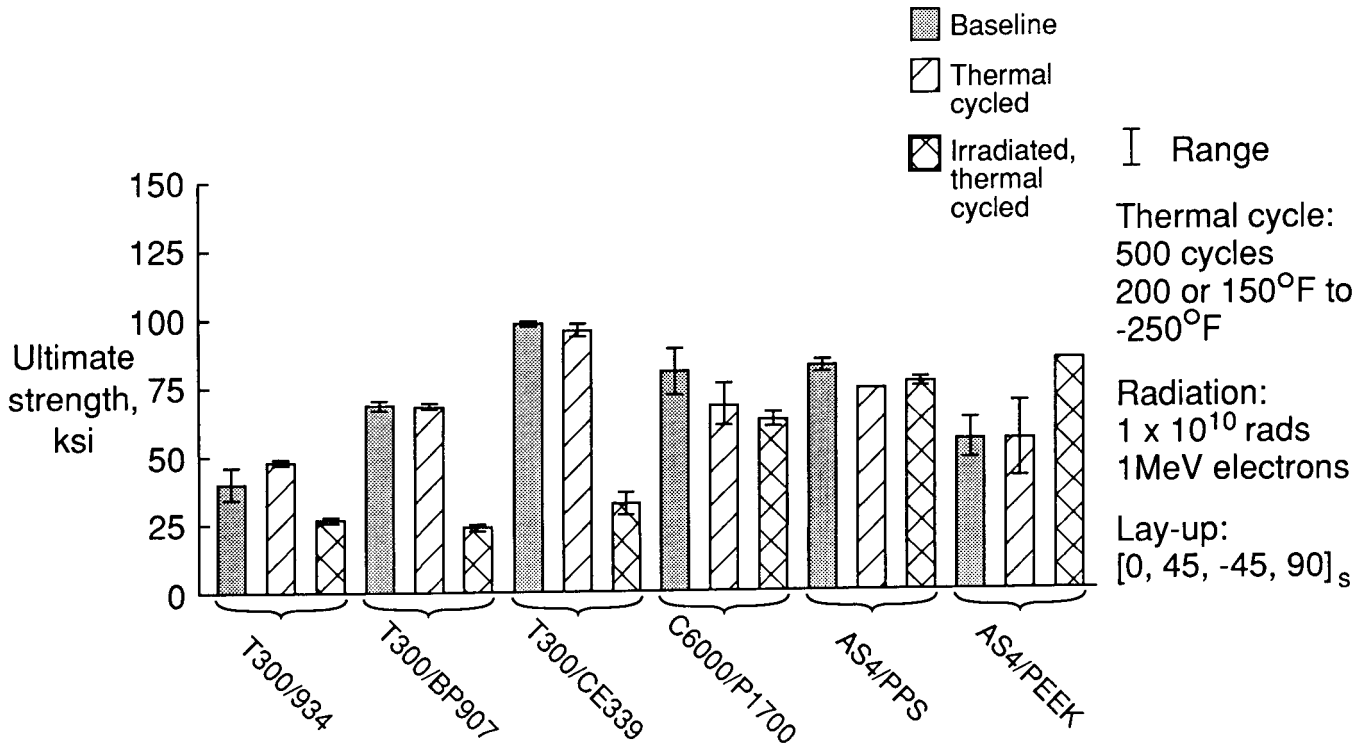

Figure 41. Ultimate strength at room temperature of six quasi-isotropic graphite fiber composites.

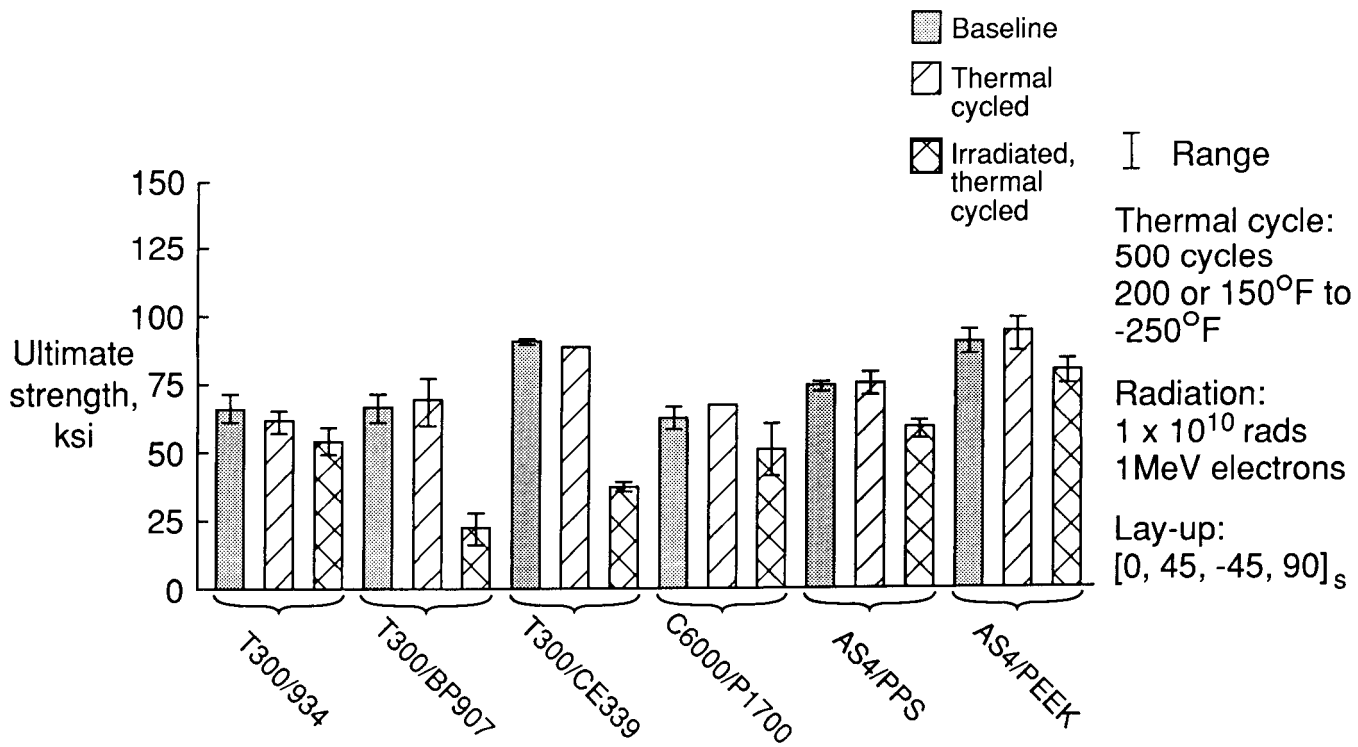

Figure 42. Ultimate strength at −250°F of six quasi-isotropic graphite fiber composites.

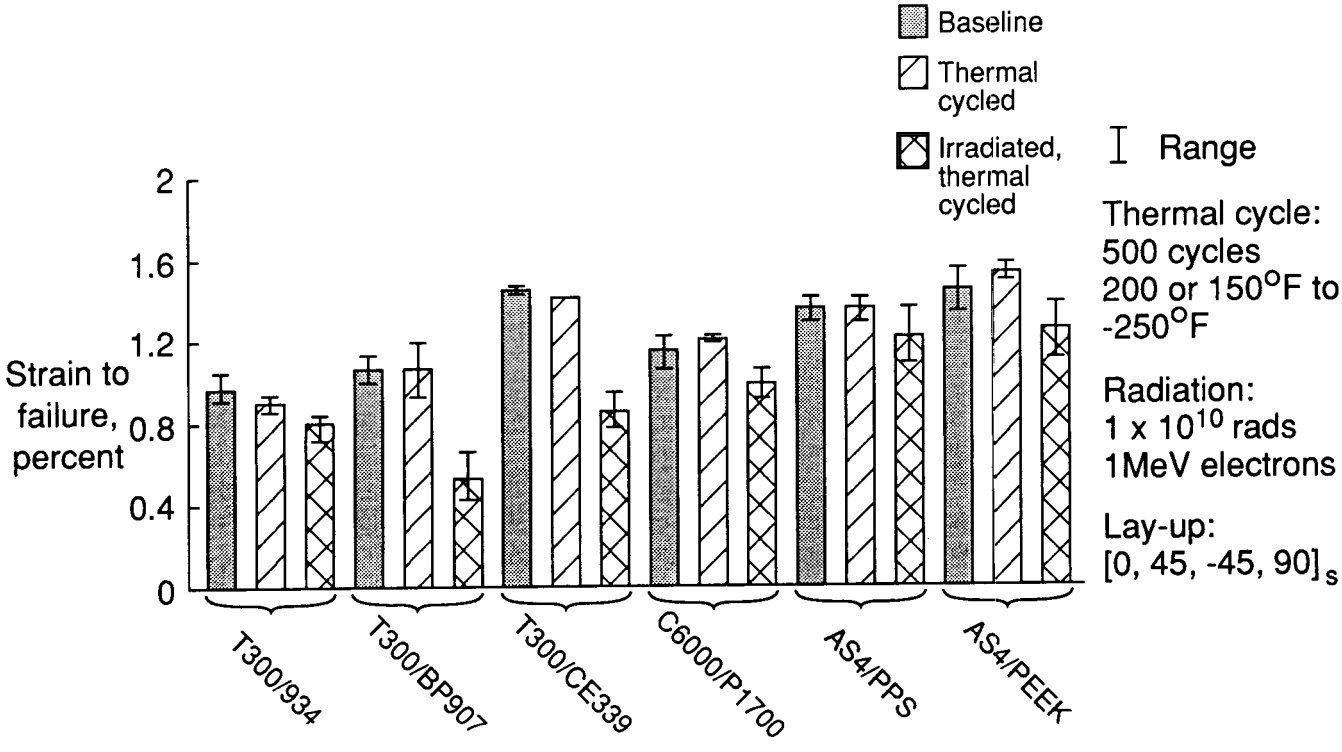

Figure 43. Failure strain at room temperature of six quasi-isotropic graphite fiber composites.

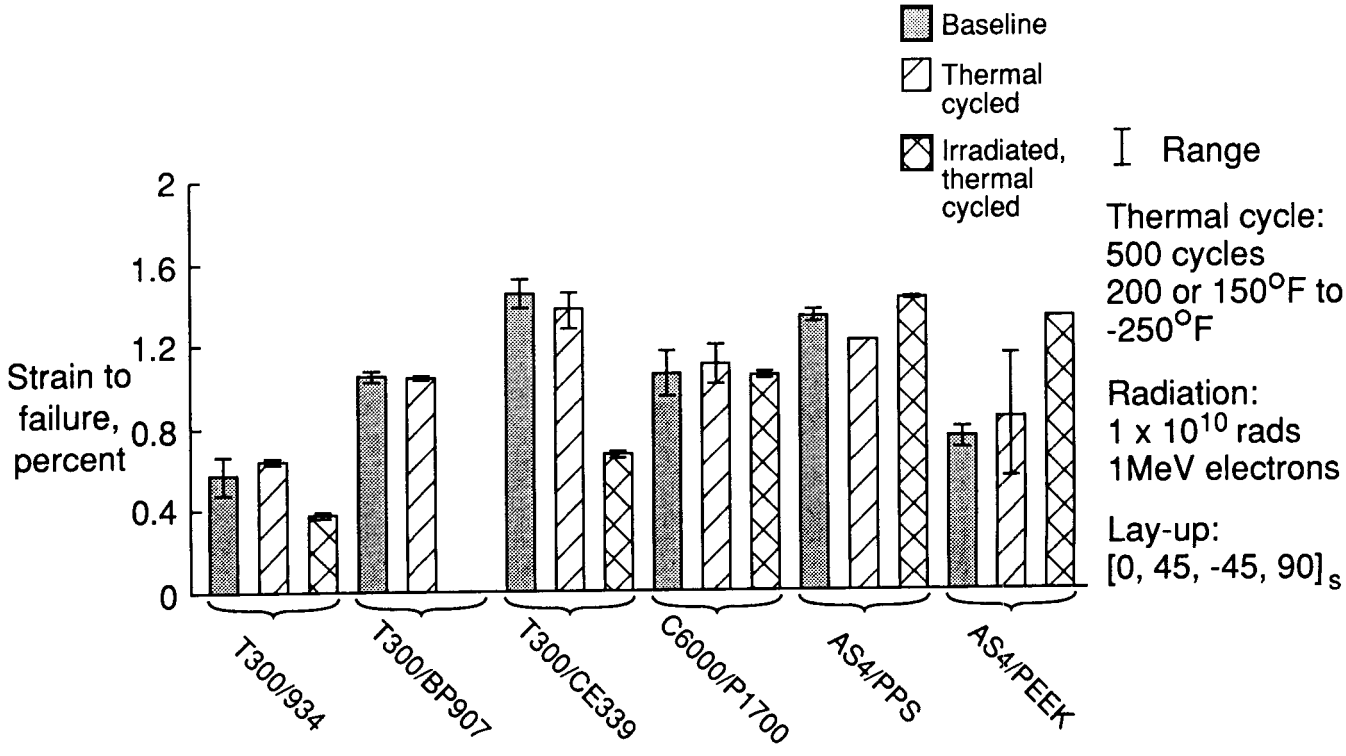

Figure 44. Failure strain at −250°F of six quasi-isotropic graphite fiber composites.

NASA
National Aeronautics and Space Administration

Report Documentation Page

1. Report No.	2. Government Accession No.	3. Recipient's Catalog No.
NASA TP-2906		

4. Title and Subtitle	5. Report Date
The Effects of Simulated Space Environmental Parameters on Six Commercially Available Composite Materials	April 1989
	6. Performing Organization Code
7. Author(s)	8. Performing Organization Report No.
Joan G. Funk and George F. Sykes, Jr.	L-16549
9. Performing Organization Name and Address	10. Work Unit No.
NASA Langley Research Center Hampton, VA 23665-5225	506-43-21-04
	11. Contract or Grant No.
12. Sponsoring Agency Name and Address	13. Type of Report and Period Covered
National Aeronautics and Space Administration Washington, DC 20546-0001	Technical Paper
	14. Sponsoring Agency Code

15. Supplementary Notes

16. Abstract

The effects of simulated space environmental parameters on microdamage induced by the environment in a series of commercially available graphite-fiber-reinforced composite materials were determined. Composites with both thermoset and thermoplastic resin systems were studied. Low-Earth-orbit (LEO) exposures were simulated by thermal cycling; geosynchronous-orbit (GEO) exposures were simulated by electron irradiation plus thermal cycling. The thermal cycling temperature range was −250°F to either 200°F or 150°F. The upper limits of the thermal cycles were different to ensure that an individual composite material was not cycled above its glass transition temperature. Material response was characterized through assessment of the induced microcracking and its influence on mechanical property changes at both room temperature and −250°F. Microdamage was induced in both thermoset and thermoplastic advanced composite materials exposed to the simulated LEO environment. However, a 350°F-cure single-phase toughened epoxy composite was not damaged during exposure to the LEO environment. The simulated GEO environment produced microdamage in all materials tested.

17. Key Words (Suggested by Authors(s))
Radiation
Thermal cycling
Composites
Thermoplastics
Thermosets
Space environment

18. Distribution Statement
Unclassified—Unlimited

Subject Category 24

19. Security Classif. (of this report)	20. Security Classif. (of this page)	21. No. of Pages	22. Price
Unclassified	Unclassified	31	A03

For sale by the National Technical Information Service, Springfield, Virginia 22161-2171